Redefining the role of Ca^{2+}-permeable channels in hereditary photoreceptor degeneration using the D- and L-cis enantiomers of diltiazem

Soumyaparna Das[1], Valerie Popp[2], Michael Power[1,3], Kathrin Groeneveld[2,4], Christian Melle[4], Luke Rogerson[3], Marlly Achury[1], Frank Schwede[5], Torsten Strasser[1], Thomas Euler[1,3], François Paquet-Durand[1*] and Vasilica Nache[2*]

[1] Institute for Ophthalmic Research, University of Tübingen, 72076 Tübingen, Germany

[2] Institute of Physiology II, University Hospital Jena, Friedrich Schiller University Jena, 07743 Jena, Germany

[3] Werner Reichardt Centre for Integrative Neuroscience (CIN), University of Tübingen, 72076 Tübingen, Germany

[4] Biomolecular Photonics Group, University Hospital Jena, Friedrich Schiller University Jena, 07743 Jena, Germany

[5] BIOLOG Life Science Institute, 28199 Bremen, Germany

Corresponding authors *

François Paquet-Durand

Institute for Ophthalmic Research, University of Tübingen, 72076 Tübingen, Germany

E-Mail: francois.paquet-durand@uni-tuebingen.de

Vasilica Nache

Institute of Physiology II, University Hospital Jena, Friedrich Schiller University Jena, 07743 Jena, Germany

E-Mail: Vasilica.Nache@med.uni-jena.de

ABSTRACT

Hereditary degeneration of photoreceptors has been linked to over-activation of Ca^{2+}-permeable channels, excessive Ca^{2+}-influx, and downstream activation of Ca^{2+}-dependent calpain-type proteases. Unfortunately, after more than 20 years of pertinent research, unequivocal evidence proving significant and reproducible photoreceptor protection with Ca^{2+}-channel blockers is still lacking. Here, we show that both D- and L-cis enantiomers of the anti-hypertensive drug diltiazem were highly effective at blocking photoreceptor Ca^{2+}-influx, most probably by blocking the pores of Ca^{2+}-permeable channels. Yet, unexpectedly, this block neither reduced activity of calpain-type proteases, nor did it result in photoreceptor protection. Remarkably, application of the L-cis enantiomer of diltiazem even led to a strong increase in photoreceptor cell death. These findings shed doubt on the previously proposed links between Ca^{2+} and retinal degeneration and are highly relevant for future therapy development as they may serve to refocus research efforts towards alternative, Ca^{2+}-independent degenerative mechanisms.

I. INTRODUCTION

The retina harbours two different types of photoreceptors: rods and cones. Rods respond to dim light and enable night-time vision, whereas cones respond to bright daylight and enable colour vision. *Retinitis pigmentosa* (RP) is a group of hereditary diseases of the retina where a primary degeneration of rods is followed by a secondary loss of cones, eventually leading to complete blindness [1, 2]. *Achromatopsia* (ACHM) is a related disease where the genetic defect causes cone degeneration without significant rod loss [3]. Overall, hereditary retinal diseases can be caused by mutations in more than 270 identified genes (https://sph.uth.edu/retnet/sum-dis.htm#B-diseases, information retrieved in Nov. 2020). Unfortunately, most cases of hereditary retinal degeneration remain without effective treatment.

Disease-causing mutations often trigger cGMP-dependent cell death in photoreceptors [4, 5]. In both rods and cones, cGMP homeostasis is regulated by two main enzymes: guanylyl cyclase, which produces cGMP, and phosphodiesterase-6 (PDE6), which hydrolyses cGMP. In turn, cGMP activates the cyclic nucleotide-gated channel (CNGC), which is located mostly in the photoreceptor outer segment (OS) [6].

In darkness, cGMP binds and activates CNGCs, leading to an influx of Ca^{2+} and Na^{+} ions. This influx is countered by a cation efflux mediated by the Na^{+}-Ca^{2+}-K^{+}-exchanger (NCKX) in the OS and by the ATP-driven Na^{+}-K^{+}-exchanger (NKX) in the photoreceptor inner segment (IS) [7]. Under physiological conditions, NKX alone is responsible for at least 50% of photoreceptor ATP-consumption [8]. In both cell body and synapse, Ca^{2+} is extruded by the plasma membrane Ca^{2+}-ATPase (PMCA). This constant flux of cations across the photoreceptor membrane in darkness is commonly referred to as the dark current, keeping the cell in a depolarized state with a membrane potential of approx. -35 mV [9, 10]. The photoreceptor depolarization allows for activation of $Ca_V1.4$ (L-type) voltage-gated Ca^{2+}-channels (VGCCs), located in the cell body and synapse, where they mediate further Ca^{2+} influx and continuous glutamate release at the synaptic terminal [9, 10].

In light, PDE6 rapidly hydrolyses cGMP, leading to CNGC closure, Ca^{2+} decrease, and hyperpolarization of the photoreceptor due to continued activity of NCKX and NKX. This in turn closes VGCC, ending synaptic glutamate release. Independent of VGCC, in the photoreceptor cell body, low Ca^{2+} levels may trigger store-operated Ca^{2+} entry (SOCE) via Ca^{2+} release-activated channels (CRACs) [11].

Disease-causing mutations, such as loss-of-function mutations in PDE6, lead to

cGMP accumulation and exacerbated activation of CNGCs, which may result in an abnormally strong influx of Ca^{2+} into photoreceptors [12, 13]. The increased CNGC activity may keep the photoreceptors in a permanently depolarized state that triggers a sustained activation of VGCCs and further Ca^{2+} influx [14]. Excessive Ca^{2+} in RP animal models, such as in the *Pde6b* mutant *rd1* and *rd10* mice [15], is thought to lead to high activity of Ca^{2+}-dependent calpain-type proteases and may precede cell death [16, 17].

To elucidate what the roles of CNGC and VGCC are in photoreceptor cell death, the *rd1* mouse was previously crossbred with knockouts (KO) that impaired the function of either CNGC (*Cngb1*$^{-/-}$) or VGCC (*Cacna1f*$^{/-}$). In the *rd1* * *Cngb1*$^{-/-}$ double mutant mouse, an animal in which both PDE6 and CNGC were dysfunctional, calpain activity was strongly reduced, and photoreceptor degeneration was considerably delayed, when compared to the single-mutant *rd1* situation [12]. Similar results were obtained when *rd10* mice were crossed with *Cngb1*$^{-/-}$ animals [18]. In contrast, in *rd1* * *Cacna1f*$^{/-}$ double-mutants, the dysfunction of the synaptic VGCCs had essentially no effect on the *rd1* degeneration [19]. However, *rd1* * *Cacna1f*$^{/-}$ double-mutants did display a marked reduction of photoreceptor calpain activity, like their *rd1* * *Cngb1*$^{-/-}$ counterparts. Taken together, these studies suggest CNGC activity as a possible driver of *rd1* photoreceptor degeneration and as a potential target for pharmacological inhibition.

Many studies over the past two decades have assessed the protective potential of Ca^{2+}-channel blockers in photoreceptor degeneration (reviewed in [20]). Here, diltiazem stands out as particularly interesting, because its D-cis enantiomer blocks VGCCs, while the L-cis enantiomer acts more strongly on CNGCs [21, 22]. Both D- and L-cis-diltiazem have been suggested to delay *rd1* photoreceptor degeneration [25, 26, 16]. However, several other studies reported conflicting or contradictory results [25, 26, 27, 28]. The reasons for this diversity in results are still unclear. Moreover, while the effect of diltiazem on VGCCs was already the topic of several studies [21-24], the direct action of diltiazem on photoreceptor CNGCs was not yet systematically characterized.

Here, we assessed the effect of D- and L-cis-diltiazem on rod and cone CNGCs heterologously expressed in *Xenopus* oocytes under physiological and RP/ACHM-like conditions. Our results suggest that only L-cis-diltiazem efficiently reduces the activity of CNGC under pathologically high cGMP-conditions, most probably by obstructing its conductive pore. This inhibitory effect of L-cis-diltiazem was voltage- and cGMP-dependent and much stronger on rod than on cone CNGCs. Surprisingly, in organotypic retinal explant cultures, derived from *rd1* mice, treatment with neither D- nor L-cis-

diltiazem prevented photoreceptor degeneration. Quite the contrary, CNGC inhibition with L-cis-diltiazem in fact exacerbated *rd1* photoreceptor loss. In summary, our results indicate that CNGC or VGCC inhibition can effectively reduce photoreceptor Ca^{2+} levels, however, this will not decrease, but may rather increase, photoreceptor cell death. This suggests that photoreceptor degeneration is largely independent of CNGC or VGCC activity.

II. RESULTS

Differential effects of D- and L-cis-diltiazem on photoreceptor CNGC

For a direct assessment of the effects of D- and L-cis-diltiazem on retinal CNGCs, we expressed the heterotetrameric rod CNGA1:B1a- and cone CNGA3:B3-channels in *Xenopus laevis* oocytes and examined their functional characteristics in inside-out membrane patches, using electrophysiological recordings. We started by confirming the correct assembly of heterotetrameric CNGC in the oocyte plasma membrane via two different tests: (1) Co-expression of the main subunits, rod CNGA1 and cone CNGA3, together with the modulatory subunits, CNGB1a and CNGB3, respectively, led to a strong increase of cAMP efficacy in heterotetrameric *vs*. homotetrameric channels, as previously reported [25, 26] (see METHODS and Supplementary Fig. 1a,b). (2) Expression of heterotetrameric CNGCs with GFP-labelled CNGB1a or CNGB3 subunits and staining the oocyte plasma membrane from the extracellular side with fluorescently-labelled lectin (Alexa Fluor™ 633 - WGA) led to spatial overlap between the GFP- and the WGA-fluorescence profiles (see METHODS and Supplementary Fig. 1c, d).

To characterize retinal CNGCs, we first measured the steady-state concentration-activation relationships in the presence of cGMP at -35 mV (Table 1; Supplementary Fig. 1e, f). The effect of diltiazem on CNGCs was tested by measuring and comparing the cGMP-induced currents in the presence and absence of either 25 or 100 µM, D- and L-cis-diltiazem, respectively (Fig. 1).

Under physiological conditions, at -35 mV and with up to 5 µM cGMP [27, 28], CNGC activity reached ~6 % of its maximum for the cone and ~1 % for the rod isoforms (yellow areas in Fig. 1a-d). When applied to the intracellular side of the membrane patch, neither D- nor L-cis-diltiazem (up to 100 µM) significantly influenced physiological CNGCs activity (Fig. 1, for statistics see Table 2). To test this finding in cone CNGC, in which under early RP-conditions a healthy cGMP homeostasis is expected, we additionally recorded and compared, within the same measurement, the CNGC currents in the presence of either cGMP or cGMP and 25 µM intracellular L-cis-diltiazem (Supplementary Fig. 2). Under these conditions, we observed no significant difference between the channel activity with and without L-cis-diltiazem.

In the presence of saturating cGMP (3 mM), both diltiazem enantiomers showed a clear inhibitory effect on cone and rod CNGCs (grey areas in Fig. 1a-d). The strongest inhibitory effect on both CNGC isoforms was triggered by L-cis-diltiazem. The rod CNGC

isoform was the most sensitive to both D- and L-cis-diltiazem (Fig. 1e). Specifically, 100 µM L-cis-diltiazem blocked ~92% of the rod CNGC activity, whereas D-cis-diltiazem at the same concentration blocked only ~36% (Table 2). In comparison, the activity of cone CNGCs was reduced by ~43% with 100 µM L-cis-diltiazem and only by ~11% with 100 µM D-cis-diltiazem. 100 µM D- and L-cis-diltiazem triggered slightly stronger inhibitory effects than those induced by 25 µM. At 100 µM cGMP, a pathologically high cGMP concentration, which emulates RP-like conditions, the diltiazem effect on rod CNGCs, mirrored very closely our observations in the presence of 3 mM cGMP (Fig. 1f).

We next measured the inhibitory effect of diltiazem on CNGCs at different voltages (-100 and +100 mV). Both diltiazem enantiomers showed a stronger inhibitory effect at depolarizing than at hyperpolarizing membrane voltages (Supplementary Figs. 3-5; Table 2). With 100 µM D-cis-diltiazem and saturating cGMP (3 mM cGMP), we observed an increase by a factor of ~4 in the strength of the cone CNGC block at +100 mV, in comparison with that at -100 mV. Under the same conditions, the inhibitory effect on rod CNGCs was increased by a factor of ~7. In comparison, the voltage dependence of the L-cis-diltiazem-induced effect was much weaker: ~2.6 times stronger block at +100 mV than that at -100 mV for cone CNGC, and only ~1.4 times for rod CNGC. In the presence of 25 µM D- or L-cis-diltiazem, we observed a similar voltage dependence of the inhibitory effects as with 100 µM (Supplementary Fig. 5).

To assess the effect of diltiazem on the channel's apparent affinity, we compared the EC_{50}-values and the Hill coefficients (H) obtained from the fits of the respective concentration-activation relationships. Under all experimental conditions, we observed a voltage-dependent decrease in the channel's apparent affinity with a maximum at +100 mV (Table 1, Supplementary Fig. 5c, d; for statistical analysis see Supplementary Table 1). In addition, diltiazem, mostly at 100 µM, triggered a systematic decrease of the H-values at both -100 and +100 mV. The similarity between the effects of D and L-cis-diltiazem on EC_{50}- and H-values, may suggest that both diltiazem enantiomers influence the apparent affinity of the CNGCs and the cooperativity between their subunits through a similar mechanism.

In conclusion, our data so far showed that (1) under physiological conditions, neither D- nor L-cis-diltiazem affect the activity of CNGCs, at the tested concentrations; (2) at saturating cGMP concentration, D- and L-cis-diltiazem had a differential inhibitory effect, with a stronger inhibition of rod- *vs.* cone-CNGCs and the effect of L- exceeding that of D-cis-diltiazem; (3) the D- and L-cis-diltiazem effects on CNGCs were strongly voltage dependent, with a maximum at depolarizing voltages.

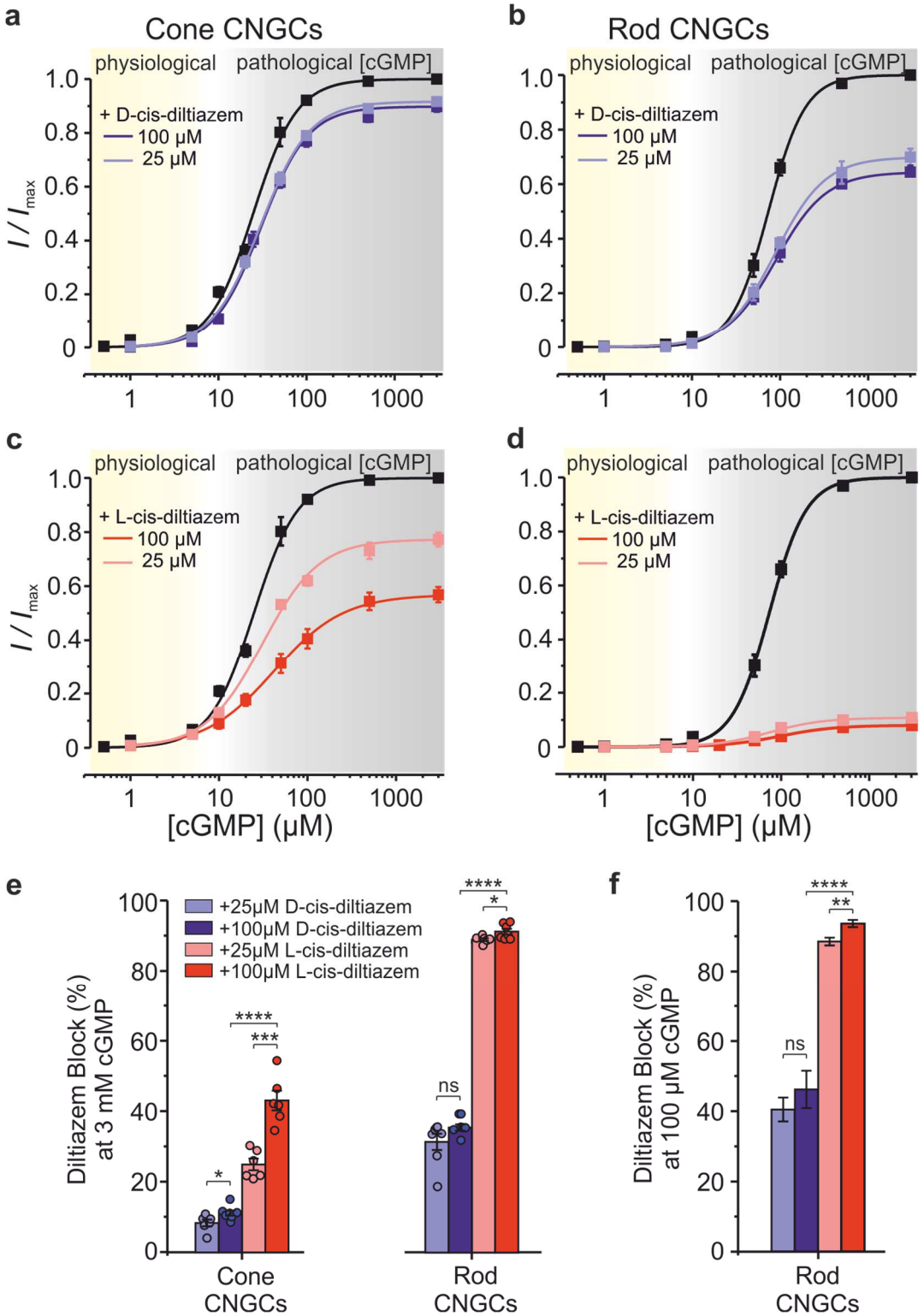

Fig. 1: Effects of D- and L-cis-diltiazem on the activity of rod and cone CNGCs. (**a-d**) Concentration-activation relationships for heterotetrameric cone (**a, c**) and rod (**b, d**) CNGCs in the presence of either 100 µM or 25 µM D- or L-cis-diltiazem, respectively, measured at -35 mV. The respective curves represent fits of the experimental data points with the Hill equation (Eq. 1). Black symbols show the normalized cGMP-triggered current amplitudes in the absence of diltiazem and are shown to point out the effect of the blocker. Light- and dark-blue symbols represent data obtained in the presence of D-cis-diltiazem, at 25 and 100 µM, respectively (**a, b**). Light- and dark-red symbols represent data obtained in the presence of L-cis-diltiazem at 25 and 100 µM, respectively (**c, d**). (**e, f**) D- and L-cis-diltiazem - block (%, ±SEM) of CNGCs in the presence of 3 mM (**e**) and 100 µM cGMP (**f**), respectively. The amount of diltiazem block was calculated using Eq. 2 (see METHODS). The respective symbols represent single measurements (see also Table 1 and 2).

	cone CNGC														
mV	**cGMP (µM)**			**+ 25µM D-cis-diltiazem**			**+100 µM D-cis-diltiazem**			**+25µM L-cis-diltiazem**			**+100 µM L-cis-diltiazem**		
	EC_{50}	*H*	n	EC_{50}	*H*	n	EC_{50}	*H*	n	EC_{50}	*H*	n	EC_{50}	*H*	n
-35	26.0 ±2.9	1.81 ±0.1	7	31.7 ±1.6	1.71 ±0.1	6	28.8 ±1.4	1.54 ±0.1	7	31.1 ±1.1	1.36 ±0.09	5	42.6 ±4.0	1.28 ±0.1	6
-100	20.7 ±2.1	2.12 ±0.1	9	28.0 ±0.6	1.93 ±0.08	8	32.5 ±3.0	1.56 ±0.1	5	28.0 ±1.2	1.65 ±0.07	10	47.8 ±6.6	1.13 ±0.09	5
+100	13.5 ±3.2	1.70 ±0.1	5	27.5 ±1.7	1.43 ±0.1	7	49.9 ±6.0	1.20 ±0.05	5	40.6 ±4.9	1.13 ±0.1	9	56.1 ±9.9	0.95 ±0.1	5
	rod CNGC														
-35	70.1 ±5.3	1.74 ±0.1	7	85.7 ±8.8	1.71 ±0.1	7	95.4 ±9.2	1.68 ±0.1	6	79.2 ±8.1	1.49 ±0.2	5	103.2 ±12.4	1.28 ±0.1	6
-100	61.5 ±5.3	1.98 ±0.1	10	86.3 ±6.4	1.93 ±0.08	5	77.2 ±5.5	1.84 ±0.08	7	84.3 ±8.8	1.27 ±0.1	5	92.4 ±15.2	1.20 ±0.1	6
+100	46.5 ±6.5	2.02± 0.07	10	109.5 ±10.0	1.43 ±0.1	6	102.8 ±7.9	1.19 ±0.2	6	134.5 ±14.8	1.18 ±0.06	5	129.3 ±13.3	1.15 ±0.1	6

Table 1: Effect of D- and L-cis-diltiazem on the apparent affinity of rod and cone CNGC. The EC_{50}-values and Hill coefficients (*H,* ±SEM) were obtained from the concentrations-activation relationships presented in Fig. 1 and Supplementary Figs. 3,4, for rod and cone CNGCs (n = number of experiments). Two-tailed unpaired Student *t*-test was used to compare the EC_{50}- and *H*-values in the presence of diltiazem with the ones obtained in its absence (Supplementary Table 1).

mV	Diltiazem Block (%) of cone CNGC at 3 mM cGMP					
	+ 25 µM D-cis-diltiazem	+ 100 µM D-cis-diltiazem	*p*-value	+ 25 µM L-cis-diltiazem	+ 100 µM L-cis-diltiazem	*p*-value
-35	8.37 ± 0.97	11.2 ± 1.1	0.0378	25.0 ± 1.6	43.2 ± 2.8	0.0002
-100	1.20 ± 0.3	8.02 ± 1.7	0.0001	4.9 ± 0.8	25.3 ± 3.4	<0.0001
+100	13.5 ± 1.6	34.0 ± 1.1	< 0.0001	39.2 ± 2.2	67.2 ± 1.4	<0.0001
	Diltiazem Block (%) of rod CNGC at 3 mM cGMP					
-35	31.5 ± 2.3	35.6 ± 0.9	ns	89.2 ± 0.37	91.5 ± 0.8	0.0270
-100	3.26 ± 1.7	11.9 ± 0.9	0.0006	52.4 ± 2.7	66.2 ± 2.0	0.0025
+100	53.5 ± 1.6	83.1 ± 1.2	<0.0001	90.0 ± 0.65	93.5 ± 1.4	0.0004
	Diltiazem Block (%) of rod CNGC at 100 µM cGMP					
-35	40.4 ± 3.4	46.1 ± 5.3	ns	88.4 ± 1.1	93.5 ± 1.1	0.0021

Table 2: Effect of D- and L-cis-diltiazem on the current amplitude of rod and cone CNGCs. The amount of block was determined by comparing the CNGC currents in the presence and in the absence of either D- or L-cis-diltiazem (±SEM, n=5-10) and was calculated using Eq. 2. The comparison between 25 and 100 µm of D- and L-cis-diltiazem, respectively, was performed using the two-tailed unpaired Student's *t*-test.

Effects of D- and L-cis-diltiazem on CNGC activation and deactivation kinetics

To characterize the effect of D- and L-cis-diltiazem on the channel's gating kinetics, we studied the activation and deactivation time courses for cone and rod CNGCs, with and without diltiazem (Fig. 2a, b; METHODS). When applying both cGMP and diltiazem simultaneously, the blocking effect took place only after channel activation. This implies that either diltiazem can block open channels only or that the blocking mechanism is slower or starts with a certain delay, reaching a maximum only after channel activation. When cGMP and diltiazem were simultaneously removed, we observed a delay of the channel's deactivation, suggesting that the channels cannot close until diltiazem is at least partially removed, as it would be the case if diltiazem blocks the channel pore. The small current increase observed during washout onset mirrors the initial phase of the diltiazem removal. The activation of CNGC (τ_{act}) seemed unaffected whereas the channel's deactivation (τ_{deact}) was delayed and slowed down by a factor of ~2 for both CNGC isoforms (Table 3). Moreover, the kinetics of the blocking event was similar for both channel isoforms (τ_{block}) (Fig. 2c, for detailed statistics see Table 3). In conclusion, only the deactivation of rod and cone CNGC was influenced by diltiazem and the effects triggered by the two diltiazem enantiomers were comparable. These findings suggest a common blocking mechanism for D- and L-cis-diltiazem, possibly by obstructing the channel pore.

Based on this hypothesis, we tested whether the observed diltiazem-induced block is obstructed by Ca^{2+}, as one of the permeating ions through CNGCs [29, 30]. To this end, we studied the effect of 25 µM L-cis-diltiazem on rod CNGCs in the presence of 1 mM $CaCl_2$ on the extracellular side of the membrane. As expected, in the presence of Ca^{2+} we found a reduced cGMP-triggered activation of CNGCs (Supplementary Fig. 6a), an effect that is consistent with a very slow Ca^{2+} permeation through the channel pore [31]. Nevertheless, the influence of extracellular Ca^{2+} on the strength of the L-cis-diltiazem-induced block was negligible (Supplementary Fig. 6b), arguing against the possibility that Ca^{2+} substantially obstructs diltiazem binding to its binding pocket. A similar result was reported earlier when studying the effect of diltiazem on the Ba^{2+}-current carried by VGCCs [21].

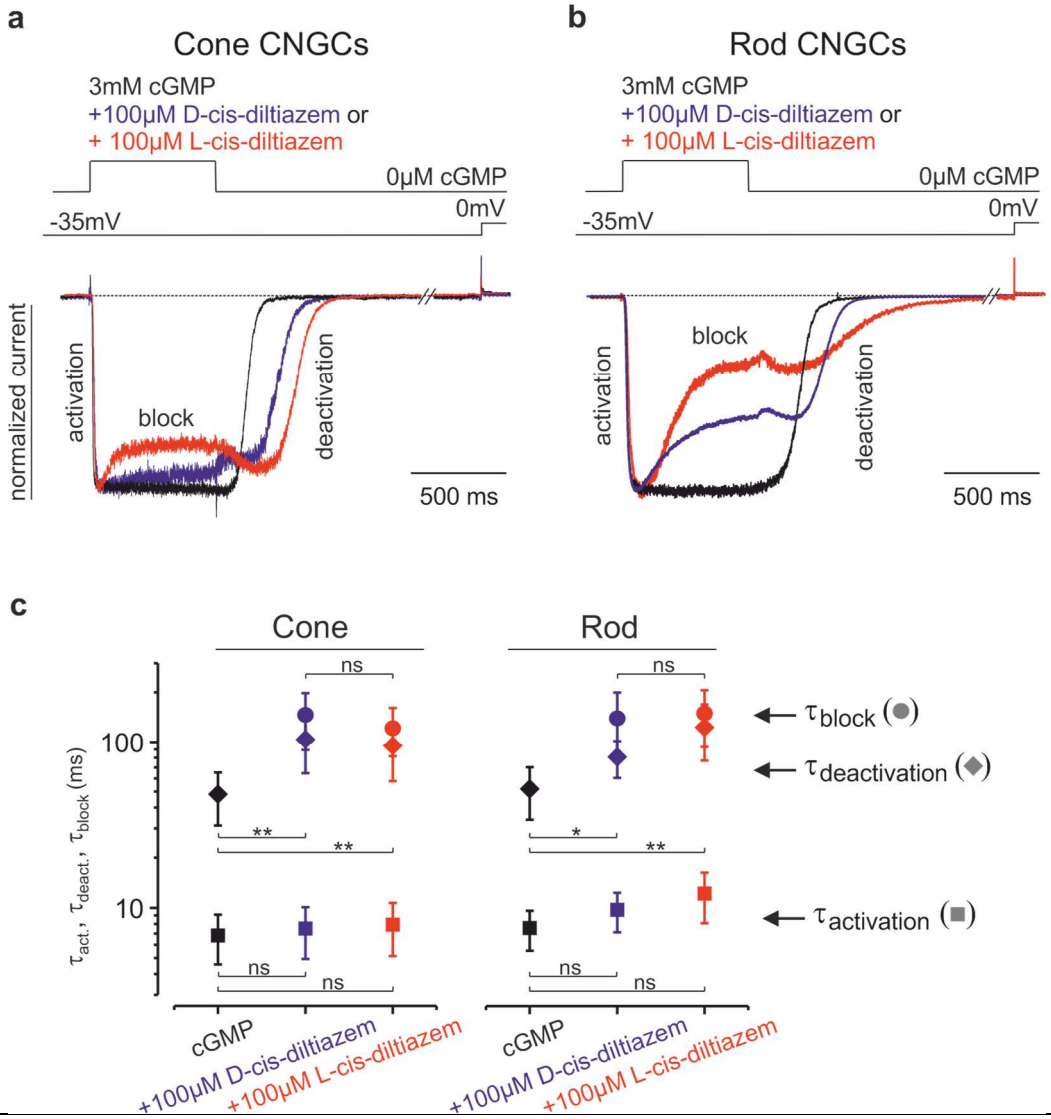

Fig. 2: D- and L-cis-diltiazem influence the gating kinetics of rod and cone CNGCs. Superimposition of representative activation-, deactivation- and block- time courses following a concentration jump from 0 µM cGMP to either 3 mM cGMP or 3 mM cGMP +

100 µM D- or L-cis-diltiazem and back to 0 µM cGMP for cone (**a**) and rod (**b**) CNGCs (n=5-9). Panels (**a**) and (**b**) show representative current traces. The current traces (blue for D-, red for L-cis-diltiazem) were normalized to the initial current level triggered by 3 mM cGMP (black) in the absence of diltiazem. Above the current traces are depicted the experimental protocols. **c**) CNGC-activation, -deactivation and -block time constants (τ_{act}, τ_{deact}, τ_{block}). The respective traces in **a**) and **b**) were fitted with mono-exponential functions (Eq. 3) and the obtained mean time constants and statistical analysis (ms, ±SEM) were included in Table 3. The time course of channel deactivation was fitted starting after the initial delay due to diltiazem removal.

	cone CNGC					
	τ_{act} (ms)	*p*-value	τ_{deact} (ms)	*p*-value	τ_{block} (ms)	*p*-value
cGMP (µM)	6.8 ± 2.3	-	48.2 ± 17.0	-		-
+ 100 µM D-cis-diltiazem	7.5 ± 2.6	ns	103.6 ± 39.1	0.0009	154.4 ± 53.4	ns
+ 100 µM L-cis-diltiazem	7.9 ± 2.8	ns	94.7 ± 36.8	0.0032	120.4 ± 38.5	
	rod CNGC					
cGMP (µM)	7.6 ± 2.1	-	52.1 ± 18.2	-		-
+ 100 µM D-cis-diltiazem	9.8 ± 2.6	ns	81.2 ± 30.5	0.0315	139.7 ± 60.2	ns
+ 100 µM L-cis-diltiazem	12.2 ± 4.1	ns	123.4 ± 46.1	0.0010	150.0 ± 56.7	

Table 3: Effect of D- and L-cis-diltiazem on the gating kinetics of cone and rod CNGCs. The effect of diltiazem on the cone and rod activation- and deactivation- time constants (τ_{act}, τ_{deact} and τ_{block}) in the presence of 3 mM cGMP (ms, ±SEM, n=5-9). Two-tailed unpaired Student *t*-test was used for the comparison between time constants obtained in the presence and in the absence of diltiazem.

Effect of L-cis-diltiazem on cGMP binding

To assess whether diltiazem influences ligand binding, we measured cGMP binding and CNGC activation, simultaneously, under steady-state conditions, with and without diltiazem, by means of confocal patch-clamp fluorometry (cPCF) [32-34]. For these experiments, we used (a) rod CNGC, the most diltiazem-sensitive channel, (b) L-cis-diltiazem, the enantiomer with the strongest blocking effect and (c) f*cGMP (8-[DY-547]-AHT-cGMP), a fluorescent derivative of cGMP (Fig. 3). In a previous study, we showed that f*cAMP, the correspondent fluorescent derivative of cAMP, has ~8× higher potency to open the olfactory CNGCs [35]. Similarly, 10 µM f*cGMP triggered already 87.4 ± 1.4% activation of rod CNGC, which is ~20 times more than the activation triggered by 10 µM cGMP (Fig. 3, see also Fig. 1b).

As expected, the 10 µM f*cGMP-induced current was reduced in the presence of L-cis-diltiazem to 10.8 ± 1.1%. The current recovery triggered by the blocker removal showed two phases, a fast recovery in which 38.9 ± 3.2% of the 10 µM f*cGMP-induced current was reached and a very slow phase which took several minutes (Fig. 3). To overrule possible side effects coming from f*cGMP, we used cGMP in similar control

measurements and obtained a similar biphasic CNGCs recovery (Supplementary Fig. 7). Moreover, we noticed a faster washout of the diltiazem-induced effect when the blocker and cGMP were concomitantly removed (Fig. 2a, b), compared to when diltiazem alone was removed from an open channel (Fig. 3). This can only be explained by an acceleration of the diltiazem unbinding triggered by the simultaneous channel closure.

During the application of L-cis-diltiazem and after its removal from the f*cGMP-activated CNGCs, we observed no major change in the intensity of the fluorescence signal which encodes for the total amount of bound f*cGMP. This showed that L-cis-diltiazem inhibits the CNGCs without disturbing the cGMP binding to the channels. These results support our electrophysiological data at -35 mV, where diltiazem showed only a minor effect on the apparent affinity of the channels (Supplementary Fig. 5c, d).

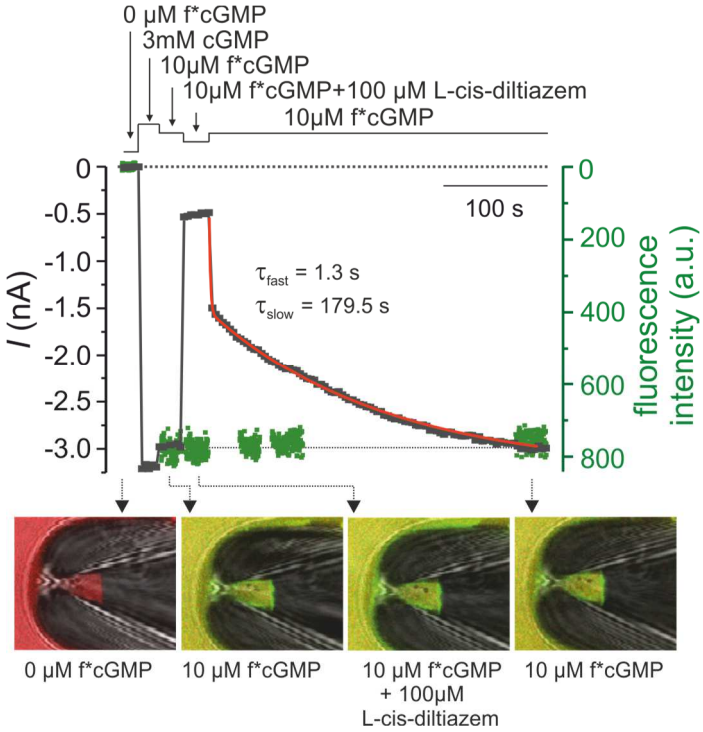

Fig. 3: L-cis-diltiazem does not influence cGMP binding to rod CNGCs. Shown is a representative cPCF measurement for studying simultaneously f*cGMP (8-[DY-547]-AHT-cGMP) binding and rod CNGCs activation in the presence of 100 µM L-cis-diltiazem. The experimental protocol is depicted above the diagram. Black symbols represent the current amplitude measured under steady-state conditions. Green symbols represent the fluorescence signal of f*cGMP which indicates the amount of ligand binding. The binding signal, measured under steady-state conditions, was normalized to the level of the 10 µM f*cGMP-induced current. In the lower part of the diagram are shown confocal images of glass pipettes, containing CNGCs-expressing membrane patches, which were obtained during the measurement in the absence (first image, left), in the presence of 10 µM f*cGMP (second and fourth image) and in the presence of 10 µM f*cGMP + 100 µM L-cis-diltiazem (third image). The time course of the current recovery upon removal of L-cis-diltiazem was fitted with a double exponential function yielding τ_{fast} = 1.5 ± 0.1 s and τ_{slow} = 161.9 ± 24.5 s (red line, n=8, Eq. 4).

Effects of D- and L-cis-diltiazem on light induced photoreceptor Ca^{2+} responses

Using two-photon Ca^{2+} imaging, we recorded light-induced cone responses in retinal slices from adult transgenic mice that had a wild-type (wt) background and expressed a fluorescent Ca^{2+} biosensor exclusively in cones [16]. As the biosensor was absent from the OS, we recorded in the cone terminal (Fig. 4a), using synaptic Ca^{2+} signals as a proxy for changes in membrane potential caused by the light-dependent modulation of CNGCs in the OS [17]. We presented series of 1-s flashes of light and measured the change (decrease) in terminal Ca^{2+}, quantifying the responses using area-under-the-curve (AUC), without (control) and in the presence of both diltiazem enantiomers at different concentrations (25, 50, and 100 µM).

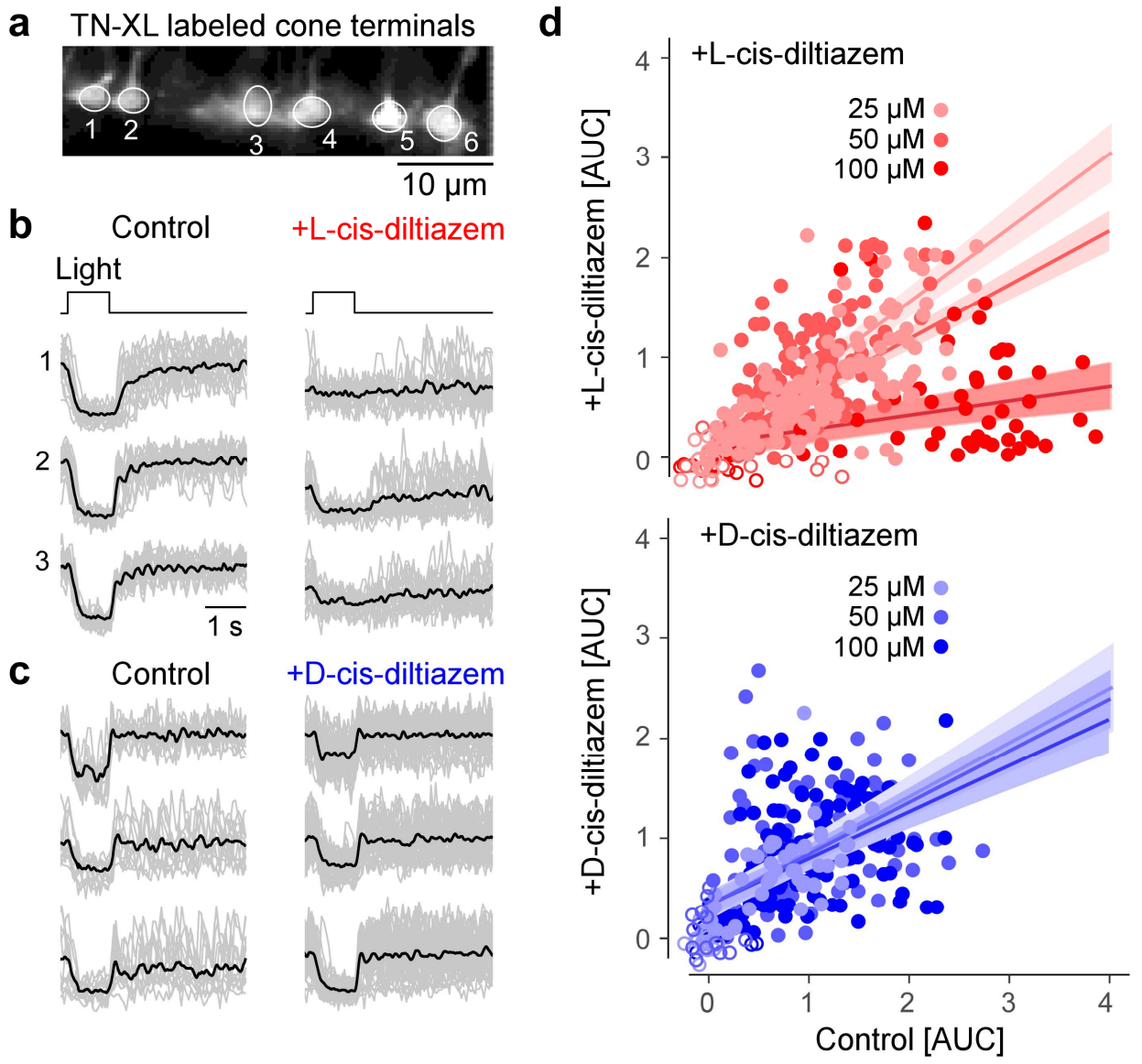

Fig. 4: Light-evoked cone Ca^{2+}-responses are reduced by L- but not by D-cis-diltiazem. (**a**) Recording light-evoked Ca^{2+}-responses from cone photoreceptor

terminals in retinal slices prepared from a transgenic mouse that expresses the fluorescent Ca^{2+} sensor TN-XL in cones. (**b, c**) Exemplary Ca^{2+} responses before (control) and in the presence of 100 µM L- (**b**) or D-cis- diltiazem (**c**) (z-scored traces; grey, single trials; black, mean of n trials, with control in (b), n=13; control in (c), n=19; L-cis-diltiazem, n=19; D-cis-diltiazem, n=38). (**d**) Scatter plot of response size (as area-under-the-curve, AUC) for both L-cis (blue; 25/50/100 µM n=137/138/61 cells) and L-cis-diltiazem (red; 25/50/100 µM n=62/140/162 cells; each data point represents a cell). Fits show mean predictions and standard errors from a multivariate linear model (METHODS and Table 4).

We used a multivariate linear model to identify which factors (*i.e.* enantiomer, concentration) are significant for predicting the response of a cell after drug treatment (for details see METHODS and Table 4). This analysis showed that L-cis-diltiazem significantly decreased the responses in a concentration-dependent manner, whereas D-cis-diltiazem did not affect the light-induced cone Ca^{2+} responses at any concentration (Fig. 4b, c, d; for detailed statistics, see Table 4). Note that L-cis-diltiazem (but not D-cis-diltiazem) also tended to decrease the Ca^{2+}-baseline level (Fig. 4b, c; left *vs*. right).

Component	*p*-value	Effect-Size	ES-Lower-CI	ES-Upper-CI
Model (all components)		0.368	0.319	0.422
AUC (control)	<0.0001	0.195	0.147	0.247
Treatment (drug)	0.00123	0.05	0.023	0.085
Treatment (concentration)	0.3416	0.039	0.016	0.072
AUC (control) x treatment (drug)	0.119	0.003	0	0.017
AUC (control) x treatment (conc.)	0.171	0.002	0	0.015
AUC (control) x treatment (drug) x treatment (conc.)	<0.0001	0.021	0.005	0.047

Table 4: Effect of D- and L-cis-diltiazem on light-evoked Ca^{2+} signals in wt cone photoreceptors. The linear modelling identified the variables that significantly predict the data. The area-under-the-curve (AUC) in the control condition was significant and had the largest effect size, with semi-partial R-squared (SPRS) equal to 0.195 ($p < 0.0001$). The drug treatment (SPRS = 0.05, $p = 0.0123$), and the drug concentration (SPRS = 0.039, $p = 0.016$) were both significant. There was also a statistically significant interaction between the AUC in the control condition, the drug treatment, and the drug concentration (SPRS = 0.021, $p < 0.0001$). Since their confidence intervals overlap, we cannot state which of these model components had the greatest effect size. There was not a significant interaction between the AUC in the control condition and the drug treatment ($p = 0.119$), or between the AUC in the control condition and the drug concentration ($p = 0.171$). (*cf*. Fig. 4; for model, see METHODS).

Taken together, these data suggested that at physiological cGMP concentrations, treatment with L-cis-diltiazem essentially locked synaptic Ca^{2+} concentrations at a low level ("constant light"), abolishing cone light responses. D-cis-diltiazem, on the other hand, had no significant effect on light-induced Ca^{2+} responses in cone photoreceptors. Since, our results on CNGCs expressed heterologously in *Xenopus* oocytes (see Fig. 1)

suggested that the rod channel isoform was more sensitive to L-cis-diltiazem than its cone counterpart, the effect of L-cis-diltiazem on rod Ca^{2+} levels is expected to be even stronger.

Expression of CNGCs in the photoreceptor outer segments

To assess the effects of Ca^{2+}-channel inhibitors on photoreceptor viability, we used wt and *rd1* mice. To ascertain that CNGC was expressed in *rd1* retina in the relevant time window, we performed immunostaining for the CNGB1a channel subunit on retinal tissue sections collected at six different time-points between post-natal day (P) 11 and 30 (Supplementary Fig. 8a-c). In addition, as the CNGB1a antibody labelled the photoreceptor OS in both genotypes, we used this staining to estimate OS length (Supplementary Fig. 8d). We found that while in wt OS length quadrupled between P11 and P30, it dramatically decreased in *rd1* retina in the same time window. As a proxy for photoreceptor degeneration, we measured the thickness of the outer nuclear layer (ONL), which contains the photoreceptor cell bodies, within a time window that includes most of the unfolding of *rd1* photoreceptor degeneration (P11 to 30). Linear mixed effect models revealed statistically significant effects of genotype and post-natal day, explaining the variability of OS length and ONL thickness data (Table 5). A Brown-Forsythe test indicated heterogeneity of variance of the fitted model residuals, however, this was not deemed to significantly affect results since linear-mixed models have been shown to be robust against this violation [36]. A post-hoc test using custom contrasts was used to compare wt and *rd1* least-square (LS) means difference between post-natal day P11 to 18, for both OS length (wt: 13.73 ± 2.05 µm; F (1, 25.25) = 44.6828; p < 0.0001, *rd1*: 3.99 ± 2.03 µm; F (1, 24.44) = 3.8582; p = 0.0610) and ONL thickness (wt: 1.46 ± 5.25 µm; F (1, 25.99) = 0.0780; p = 0.7822) *rd1*: 43.31 ± 5.13 µm; F (1, 24.18) = 71.1854; p < 0.0001).

In summary, in *rd1* retina ONL loss was correlated with a massive reduction in OS length. Nonetheless, at the beginning of the *rd1* degeneration (~P10), CNGC expression, as assessed via OS length, was still comparable to that in wt animals (average P11 OS length LS means difference between wt and *rd1* 0.18 ± 2.05 µm, F (1, 25.25) = 0.0078; p = 0.9304). This suggests that the window-of-opportunity for a treatment that targets CNGC reaches until at least P11.

	OS length n = 109, $R^2_{adj.}$ = 0.96		**ONL thickness** n = 109, $R^2_{adj.}$ = 0.93	
Fixed effect	*F*-statistic	*p*-value	*F*-statistic	*p*-value
genotype	F(1, 25.25 = 0.0078)	0.9304	F(1, 25.99) = 2.6450	0.1159

Time-point	$F(5, 24.7) = 4.4213$	0.0052	$F(5, 24.77) = 15.1946$	< 0.0001
Retinal position	$F(2, 48.36) = 0.2982$	0.7435	$F(2, 49.39) = 2.9380$	0.0623
genotype x time-point	$F(5, 24.7) = 13.2699$	< 0.0001	$F(5, 24.77) = 12.0885$	< 0.0001
genotype x retinal position	$F(2, 48.36) = 0.3245$	0.7245	$F(2, 49.39) = 0.9156$	0.4070
timepoint x retinal position	$F(10, 47.94) = 3.8401$	0.0007	$F(10, 48.41) = 2.0258$	0.0508
genotype x time-point x retinal position	$F(10, 47.94) = 4.2248$	0.0003	$F(10, 48.41) = 1.3344$	0.2397

Table 5: Effects explaining the variability of the length of OS with respect to ONL thickness in *rd1* and wt. Results of the linear mixed-effects models with the dependent variables OS length and ONL thickness. The models' residuals followed a normal distribution, while the Brown-Forsythe test indicated a violation of the assumption of homoscedasticity for both models. However, linear mixed-effects models estimates have been shown to be robust against such violations [36].

Proteolytic activity in photoreceptors after treatment with D- and L-cis-diltiazem

The influx of Ca^{2+} through CNGCs is believed to be driving the degeneration process via activation of Ca^{2+}-dependent calpain-type proteases [37]. We investigated the effects of D- and L-cis-diltiazem treatment on calpain activity, using an *in situ* activity assay on unfixed retinal tissue sections, and an immunostaining approach detecting activated calpain-2 [38]. Organotypic retinal tissue cultures derived from wt and *rd1* animals were treated with D- and L-cis-diltiazem, respectively, from P7 to P11.

In wt retina, calpain activity in general and calpain-2 activation specifically was rather low, when compared to the *rd1* situation where both markers labelled large numbers of photoreceptors in the ONL (Fig. 5a-d). In both genotypes, treatment with D-cis-diltiazem had no detectable effect on the numbers of photoreceptors positive for calpain activity or calpain-2 activation (Fig. 5e-h). Surprisingly, when retinal explants were treated with L-cis-diltiazem (Fig. 5i-l), calpain-2 activation in the ONL was significantly increased (F (1, 11.87) = 14.7372; p = 0.0024; Fig. 5i, j, n; Table 7). In conclusion, neither D- nor L-cis-diltiazem caused a statistically significant reduction of overall calpain activity (Fig. 5m, n; Tables 6, 7) in wt or *rd1* photoreceptors, even though a significant increase in calpain-2 activation was observed.

Another type of proteolytic activity, commonly associated with apoptotic cell death, is the activity of caspase-type proteases. To investigate a possible activation, the *rd1* treated and untreated retinal tissues were tested for activation of caspase-3, using an immunostaining approach with an antibody specifically directed against the active protease [39]. Under all conditions tested, caspase-3 activity was essentially undetectable in retinal sections (Supplementary Fig. 9, Table 6), thus likely ruling out an

435 important involvement of caspase activity and, by extension, of apoptotic processes in
436 retinal degeneration, with or without diltiazem treatment.

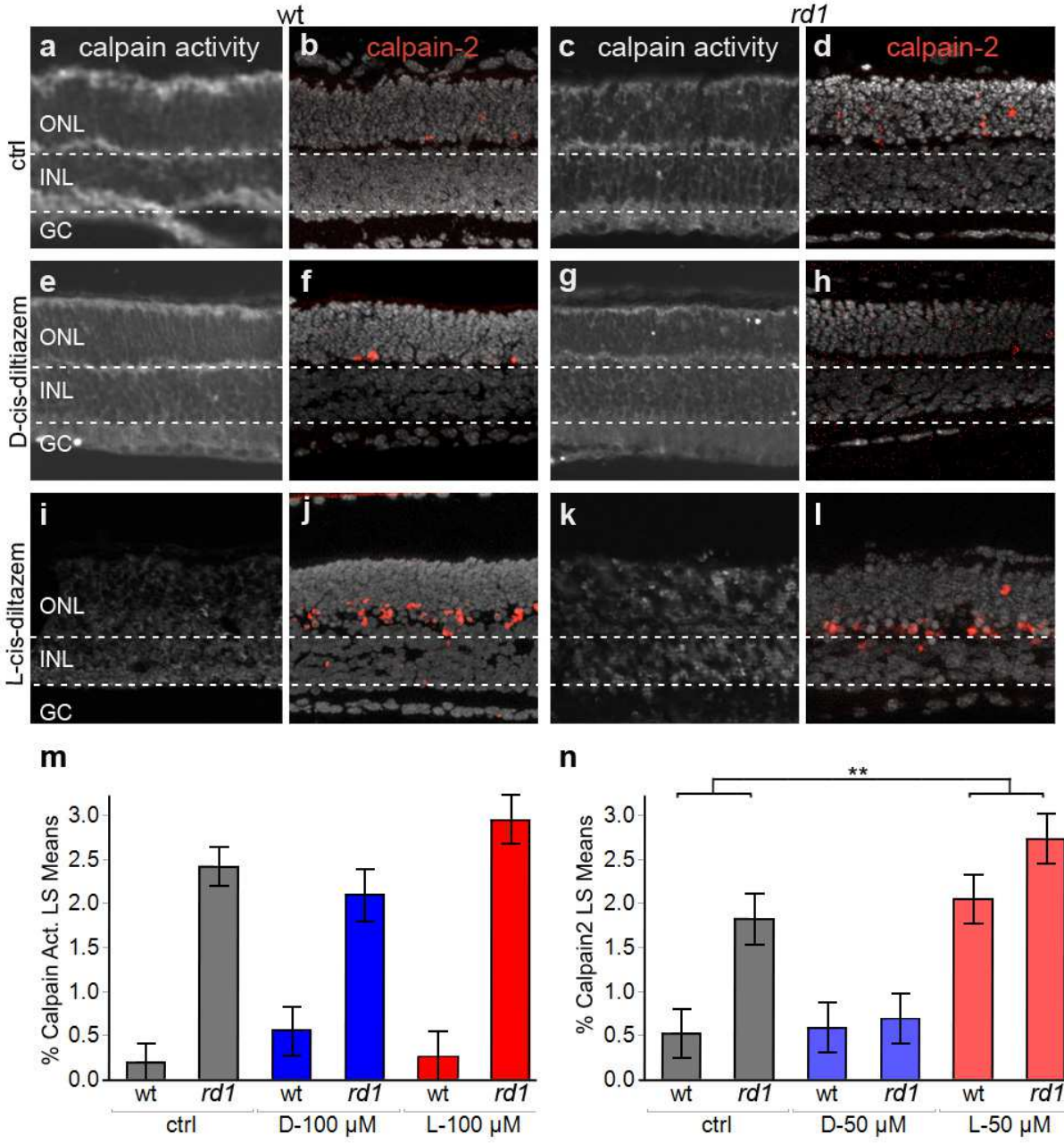

437

438

439 **Fig. 5: Effects of diltiazem treatment on calpain activity.** Calpain-activity assay and
440 immunostaining for activated calpain-2 in wt and *rd1* retina. Untreated retina (ctrl; **a-d**)
441 was compared to treatment with D-cis diltiazem (**e-h**) or L-cis diltiazem (**i-l**). The bar
442 graphs show the least-square (LS) means percentages of cells positive for calpain
443 activity (**m**) and activated calpain-2 (**n**) in wt and *rd1* retina, compared to the untreated
444 control (ctrl). Asterisks indicate a statistically significant difference from a contrast test
445 performed between control and 50 µM L-cis-diltiazem treatment (L-50 µM). For statistical
446 analysis, see Tables 6 and 7; error bars represent SEM; ** = $p < 0.01$.

447

Effect of D- and L-cis-diltiazem on *rd1* photoreceptor degeneration

To evaluate the effect of CNGC and VGCC inhibition on retinal degeneration, we used the TUNEL assay to quantify the amount of cell death in the ONL [40]. D- and L-cis-diltiazem were used to treat organotypic retinal explant cultures derived from wt and *rd1*. In additional experiments, retinal explants derived from more slowly degenerating *rd10* animals were used [37].

As expected, in the ONL of wt retinal explants a relatively low number of cells were positive for the TUNEL assay, when compared with their *rd1* counterparts (Fig. 6a, b). D-cis-diltiazem treatment did not elevate the numbers of TUNEL positive, dying cells in the wt and *rd1* ONL (Fig. 6c, d). In contrast, L-cis-diltiazem treatment (Fig. 6e, f) led to a clear increase of cell death in both wt (F (1, 21.63) = 86.7207, $p < 0.0001$) and *rd1* retina (F (1, 26.68) = 191.1994, $p < 0.0001$; Fig. 6g, h), when compared to untreated control. Quantification of the different diltiazem treatments in wt and *rd1* retina showed a significant rise in ONL cell death with L-cis-diltiazem treatment (Fig. 6g, h; for statistics see Tables 6, 7).

Interestingly, the distribution of degenerating photoreceptors within the ONL was altered by the diltiazem treatments. Typically, TUNEL positive cells in the ONL of untreated retinal explants are uniformly distributed across the whole thickness of the ONL (Fig. 6a, b). In contrast, in the cultures treated with 100 µM L-cis-diltiazem, most of the dying cells were located close to the outer plexiform layer (OPL) (Fig. 6e, f). A corresponding quantification revealed that under control conditions dying *rd1* photoreceptor distributed almost evenly within the ONL (percent *rd1* dying cells in inner half of ONL = 60 ± 3%). With D-cis-diltiazem treatment 57 ± 4% of dying cells were localized to the same space, while with L-cis-diltiazem treatment about 85 ± 3% (F (1, 10.42) = 54.2025, $p < 0.0001$; Tables 6,7) of the TUNEL positive cells were located in the lower half of the ONL (Fig. 6i).

Finally, a study on *rd10* retina yielded results similar to what was seen for the *rd1* situation: 100 µM D-cis-diltiazem had no significant effect on cell death, while 100 µM L-cis-diltiazem treatment produced a strong increase in photoreceptor cell death (F (1, 9.25) = 42.9966, $p < 0.0001$; Fig. 6j).

Taken together, our data indicate that L-cis-diltiazem treatment in wt retina was toxic to photoreceptors at all concentrations tested. Curiously, in *rd1* retina L-cis-diltiazem became toxic only at concentrations above 50 µM. In comparison, D-cis-diltiazem, up to 100 µM, did not detectably influence cell viability in either wt-, *rd1*-, or *rd10*- retinas. More

482 importantly, both diltiazem enantiomers failed to show any protective effects in *rd1* or
483 *rd10* mutant retina.

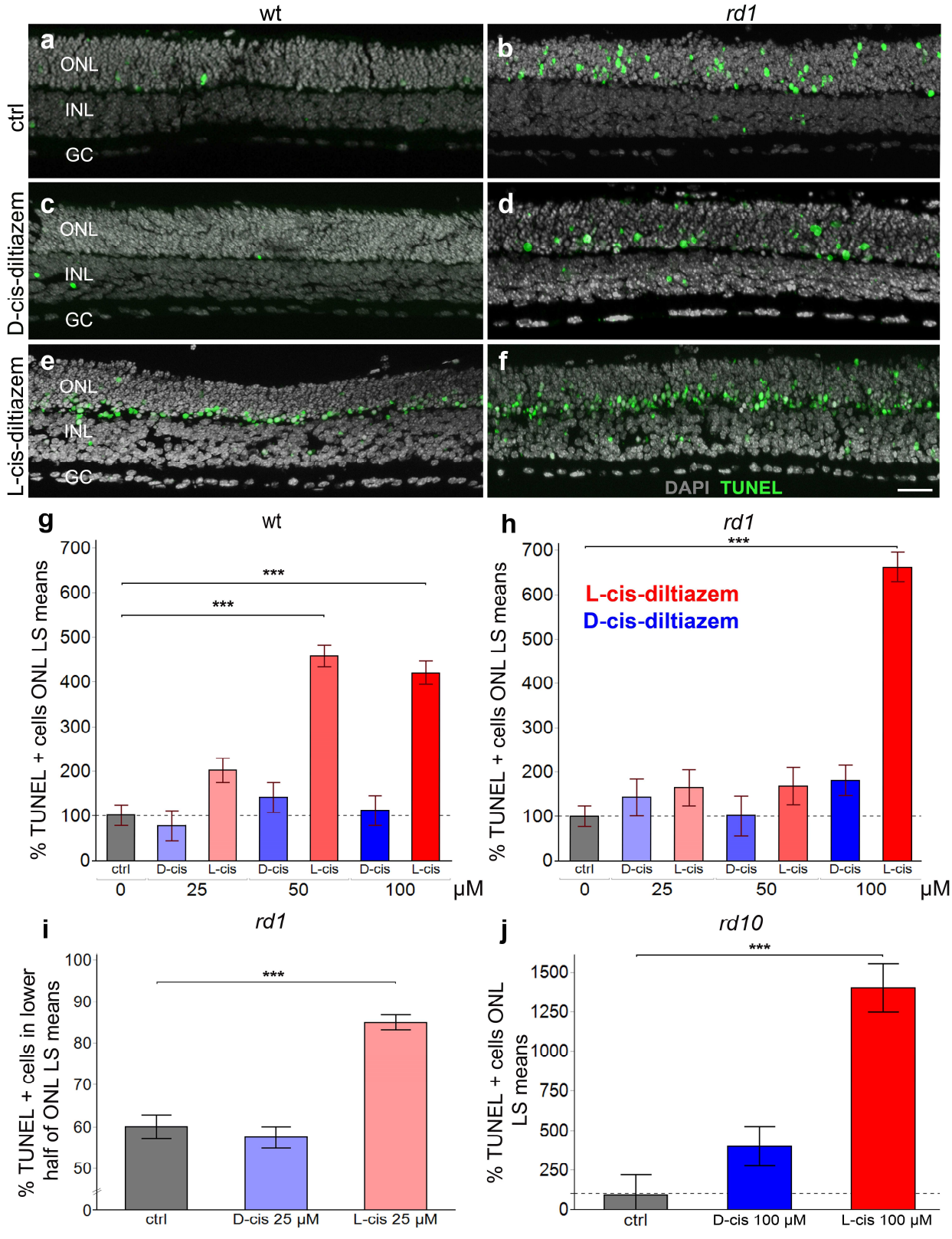

484

485 **Fig. 6: Effects of D- and L-cis-diltiazem on retinal cell viability.** The TUNEL assay
486 was used to label dying cells (green) in wt and *rd1* retinal explant cultures. DAPI (grey)
487 was used as a nuclear counterstain. Control retina (untreated; **a, b**) was compared to
488 retina treated with either 50 µM of D- (**c, d**) or L-cis-diltiazem (**e, f**). Note the large

numbers of dying cells in the *rd1* outer nuclear layer (ONL). The bar charts show the least-square (LS) means percentage of TUNEL positive cells as a function of diltiazem concentration, for wt (**g**) and *rd1* (**h**) retina, as a function of localization with respect to the outer plexiform layer (OPL) (**i**), and for *rd10* retina (**j**), respectively. In wt, *rd1*, and *rd10* retina treatment with L-cis-diltiazem strongly increased the numbers of TUNEL positive cells in the ONL. Statistical significance was analysed by post-hoc contrast test (*cf.* Table 7), errors bars represent SEM, *** = $p < 0.001$. INL = inner nuclear layer, GC = ganglion cell layer. Scale bar = 50µm.

When comparing the percentages of dying *rd1* photoreceptors cells at P11 (*i.e.* TUNEL positive cells) with the corresponding values of calpain activity positive cells, under control conditions, the ratio between these two values was 1.09 (calpain activity positive cells / TUNEL positive cells; *cf.* Figs. 5, 6). However, the D-cis-diltiazem treatment lowered this ratio ~2.5 times to 0.4, while L-cis-diltiazem treatment decreased it ~6 times to 0.17. These changes in the proportions of calpain to TUNEL positive cells indicate that intracellular Ca^{2+} levels were indeed reduced by the diltiazem treatments. However, at the same time, cell death levels either remained constant (D-cis-diltiazem) or even increased (L-cis-diltiazem), indicating that this form of cell death must be largely Ca^{2+} independent.

Dependent variable	Genotype	Fixed effect	Normality of residuals	Homo-scedasticity	*F*-statistic	*p*-value
TUNEL	wt (35) $R^2_{adj.}$ = .80 n = 336	Concentration[1]	Yes	No	$F(3, 17.92) = 20.7656$	<0.0001
		Treatment			$F(1, 303.74) = 0.171$	0.6795
		Concentration x Treatment			$F(3, 22.8) = 29.6038$	<0.0001
	rd1 (36) $R^2_{adj.}$ = .88 n = 331	Concentration[1]	Yes	No	$F(3, 24.82) = 37.8570$	< 0.0001
		Treatment			$F(1, 306.63) = 0.0787$	0.7792
		Concentration x Treatment			$F(3, 27.75) = 31.0649$	<0.0001
	rd10 (10) $R^2_{adj.}$ = .84 n = 112	Concentration[4]	Yes	No	$F(1, 8.11) = 25.9134$	<0.0009
		Treatment			$F(1, 100.96) = 0.0026$	0.9598
		Concentration x Treatment			$F(1, 10.43) = 23.5461$	<0.0006
Calpain activity	wt (11) & *rd1* (11) $R^2_{adj.}$ = .86 n = 143	Concentration[4]	Yes	No	$F(1, 16.41) = 99.2752$	<0.0001
		Treatment			$F(2, 16.41) = 0.793$	0.4691
		Concentration x Treatment			$F(2, 16.41) = 2.055$	0.1598
Calpain- 2	wt (9) & *rd1* (9) $R^2_{adj.}$ = .83 n = 117	Genotype	Yes	No	$F(1, 12.14) = 9.0927$	0.0106
		Treatment			$F(2, 12.14) = 20.2775$	0.0001
		Genotype x Treatment			$F(2, 12.14) = 2.2535$	0.1471
Caspase-3	*rd1* (11) $R^2_{adj.}$ = .04 n = 58	Treatment	Yes	Yes	$F(2, 7.15) = 0.3799$	0.6970
ONL localisation TUNEL	*rd1* (9) $R^2_{adj.}$ = .72 n = 53	Treatment	Yes	No	$F(2, 10.11) = 49.4033$	<0.0001
Treatment: {D-cis-diltiazem, L-cis-diltiazem}, [1]{0, 25, 50, 100 µM}, [2]{0, 25 µM}, [3]{0, 50 µM}, [4]{0, 100 µM}						

Table 6: Data analysis using linear mixed-effects models. Shown are the effects that

explain the variability of the dependent variables TUNEL, calpain activity, calpain-2 positive cells, as well as localization of TUNEL positive cells within the ONL. All models included the animal as a random effect to account for repeated measures. Numbers in brackets indicate the total number of animals used per genotype, n represents the number of observations used in the model. Normality of residuals was assessed visually; heterogeneity of residual variances (homoscedasticity) was tested with the Brown-Forsythe test. Linear mixed-effects models have been shown to be robust against violations of model assumptions.

	Contrast LS means [95% confidence interval] (%)		LS means diff. ± SE (%)	F-statistic	*p*-value
ONL localisation TUNEL	*rd1* ctrl 59.98 [54.04, 65.92]	*rd1* D-25 µM 57.44 [52.05, 62.83]	2.54 ± 3.79	F(1, 16.33) = 0.4511	0.5112
		rd1 L-25 µM 85.03 [79.70, 90.36]	25.05 ± 3.40	F(1, 10.42) = 54.2025	< 0.0001
Calpain-2	*rd1* ctrl 1.82 [1.20, 2.44]	*rd1* D-50 µM 0.68 [0.07, 1.30]	1.13 ± 0.40	F(1, 12.52) = 7.9008	0.0152
		rd1 L-50 µM 2.73 [2.11, 3.35]	0.91 ± 0.40	F(1, 12.69) = 5.0979	0.0423
	wt ctrl 0.52 [0.09, 1.13]	wt L-50 µM 2.04 [1.43, 2.66]	1.52 ± 0.39	F(1, 11.87) = 14.7372	0.0024
TUNEL	*rd1* ctrl 98.10 [50.88, 145.32]	*rd1* D-100 µM 180.85 [111.06, 250.63]	82.75 ± 41.14	F(1, 28.11) = 4.0454	0.0540
	rd1 ctrl 101.96 [54.54, 149.38]	*rd1* L-100 µM 661.96 [593.66, 730.26]	560.00 ± 40.99	F(1, 26.68) = 191.1994	<0.0001
	rd10 ctrl 90.68 [201.44, 382.81]	*rd10* D-100 µM 401.33 [111.58, 691.07]	310.60 ± 178.75	F(1, 8.10) = 3.0200	0.1200
	rd10 ctrl 93.60 [198.61, 385.80]	*rd10* L-100 µM 1403.14 [1060.80, 1745.48]	1310.00 ± 199.71	F(1, 9.25) = 42.9966	<0.0001
	wt ctrl 105.35 [58.38, 152.32]	wt D-100 µM 112.44 [43.49, 181.39]	7.10 ± 39.87	F(1, 19.17) = 0.0316	0.8607
	wt ctrl 98.28 [51.36, 145.21]	wt L-50 µM 458.14 [406.36, 509.93]	359.90 ± 33.31	F(1, 18.59) = 116.6931	<0.0001
		wt L-100 µM 420.42 [366.06, 474.78]	322.10 ± 34.59	F(1, 21.63) = 86.7207	<0.0001

Table 7: Post-hoc analysis of the linear mixed-effects models. Results of contrast tests comparing the least-square means, which resulted from the linear mixed-effects models shown in Table 6.

III. DISCUSSION

While Ca^{2+}-permeable channels have been studied very extensively as potential targets for the therapy of retinal diseases, numerous attempts to block photoreceptor Ca^{2+}- influx for therapeutic purposes have been unsuccessful to date (reviewed in [20]). Here, we show that diltiazem enantiomers were highly effective at blocking photoreceptor Ca^{2+} influx through CNGCs at pathologically high cGMP concentrations, likely by blocking the channel's pore. Yet, unexpectedly, this block neither reduced activity of Ca^{2+} dependent calpain-type proteases, nor did it result in photoreceptor protection. These results raise the question whether Ca^{2+}-permeable channels are suitable targets for therapeutic interventions, and furthermore, whether high intracellular Ca^{2+} *per se*, can still be considered a driver of photoreceptor death.

Effect of D- and L-cis-diltiazem on photoreceptor CNGCs

Until now, in the CNGC field, diltiazem has only been used as a tool to characterize various aspects of CNGC activity or to verify the presence of heterotetrameric CNGCs in heterologous expression systems. [22, 26, 41]. Although previous studies on retinal degeneration found that the photoreceptor CNGC is one of the main targets of elevated cGMP, conclusive studies showing the efficacy of diltiazem are still missing. We characterized the effect of D- and L-cis-diltiazem on retinal CNGC isoforms heterologously expressed in *Xenopus* oocytes, under different cGMP levels, voltages, and diltiazem concentrations. We found that at physiological cGMP, neither D- nor L-cis-diltiazem showed an appreciable effect on CNGC. In the presence of high cGMP concentrations, both diltiazem enantiomers reduced CNGC activity, although L-cis-diltiazem had a much stronger inhibitory effect than D-cis-diltiazem, and this effect was stronger on rod- than on cone-CNGC.

To date electrophysiological recordings from single photoreceptors of retinal disease models are very rare [42]. Still, we may expect *rd1* rod photoreceptors to be in a permanently depolarized state due to the high CNGC activity triggered by high cGMP. We indeed found a strong voltage dependence of the diltiazem-inhibitory effect, with a maximum at depolarizing voltages. This would suggest that a disease-induced photoreceptor depolarization will amplify the diltiazem-induced inhibition of CNGCs.

D- and L-cis-diltiazem - blocking mechanism of photoreceptor CNGCs

Earlier studies on photoreceptor CNGC suggested several binding sites for diltiazem, either at the pore entrance, on the cytoplasmic side of the channel [23], or within the

channel pore, about half-way across the membrane [43]. Recently, L-cis-diltiazem was shown to block the voltage-gated Ca^{2+}-channel (bacterial CavAb and rabbit $Ca_v1.1$) by blocking its conductive pathway [44, 45]. Nevertheless, in case of CNGC, the inhibitory effect could be also due to a disturbed cGMP binding to the channel.

Herein, we investigated the effect of L-cis-diltiazem on cGMP binding to CNGCs by means of cPCF. Our data suggest that L-cis-diltiazem acts by blocking the channel pore and affecting the flow of ions across the membrane. Our conclusion is based on several observations: (1) the time delay observed between channel activation and diltiazem block, (2) the time delay observed between diltiazem removal and channel closure and the acceleration of diltiazem removal by the concomitant channel deactivation, and (3) the undisturbed cGMP binding in the presence of diltiazem. Moreover, the fast and the slow component observed during L-cis-diltiazem washout from the open channel may indicate the existence of several binding pockets within the channel's pore, with different affinities.

Although L-cis-diltiazem had only a moderate influence on the channel's deactivation kinetic, we observed a negative influence on the cooperativity between CNGC subunits. Together with the fact that L-cis-diltiazem only inhibits heterotetrameric channels [26], this suggests a direct interaction between diltiazem and the modulatory subunits, rod CNGB1a and cone CNGB3, respectively. Future studies based on molecular-docking approaches may shed new light on the exact location of the diltiazem binding site within the channel's pore and its biophysical characteristics.

An integrated view on Ca^{2+} flux in photoreceptor degeneration

Photoreceptor degeneration in hereditary retinal diseases has long been proposed to be caused by excessive Ca^{2+} influx [13, 46], sometimes referred to as the "high Ca^{2+} hypothesis". In terms of phototransduction activity this hypothesis relates to a situation of constant darkness, *i.e.* high levels of cGMP, constant activation of CNGC, and thus high Ca^{2+} levels in photoreceptor OS. However, an alternative hypothesis suggested that photoreceptor death might be triggered by too low Ca^{2+}, something that has been termed the "low Ca^{2+} hypothesis" [47].

In the following, we will discuss our data in view of what is known about Ca^{2+} fluxes in the different photoreceptor compartments (Fig. 7a), under different experimental

conditions, and will attempt to resolve some of the apparent contradictions between high and low Ca^{2+} hypotheses.

When considering possible pathological mechanisms, we must keep in mind that the phototransduction cascade itself is Ca^{2+}-modulated. For instance, in wt photoreceptors, under dark conditions (Fig. 7b), the guanylyl cyclase and therefore cGMP synthesis is inhibited by Ca^{2+} via guanylyl cyclase activating protein (GCAP) [48], the cGMP affinity of CNGC is reduced via a Ca^{2+}-calmodulin pathway [49], and the Ca^{2+} influx through VGCC can trigger a Ca^{2+}-induced release of Ca^{2+} from endoplasmic reticulum [50]. During illumination these processes are reversed, cGMP-level drops, CNGC and then VGCC close, and Ca^{2+} levels in OS and synapse decrease (Fig. 7c).

In wt retina, with relatively low cGMP levels and the CNGCs mostly closed, we expected no major CNGC inhibition by either D- or L-cis-diltiazem, as observed from the experiments on heterologously expressed channels. D-cis-diltiazem, will, however, block VGCC, reducing Ca^{2+} influx into cell body and synapse (Fig. 7d). Surprisingly, our Ca^{2+}-imaging data, obtained on wt photoreceptors, showed that L-cis-diltiazem reduced synaptic Ca^{2+} levels more strongly than D-cis-diltiazem. A reason for this observation could be a direct inhibition of synaptic VGCCs by L-cis-diltiazem (Fig. 7e). What argues against this explanation is that since D-cis-diltiazem blocks VGCC more strongly than L-cis-diltiazem [21], we should have detected an even stronger effect on wt photoreceptor synaptic Ca^{2+} levels with D-cis-diltiazem treatment. Yet, D-cis-diltiazem had almost no effect on synaptic Ca^{2+}-levels.

An alternative and perhaps more likely explanation for the unexpected effect of L-cis-diltiazem is that even the smallest inhibition of CNGC would trigger, due to the continuous NCKX-mediated Ca^{2+} efflux, a Ca^{2+}-decrease in the OS and the subsequent gradual disinhibition of guanylyl cyclase. This would raise OS cGMP, leading to stronger CNGC activation and thus to an increasingly stronger CNGC inhibition by L-cis-diltiazem. Hence, the photoreceptor would hyperpolarize, closing synaptic VGCC. The concomitant block of CNGC and lack of VGCC activation may result in a complete block of Ca^{2+} influx and hence a depletion of Ca^{2+} from intracellular stores. This may in turn cause SOCE and Ca^{2+} influx via CRAC [11] and, hence, could explain the increased calpain-2 activation observed in photoreceptor cell bodies treated with L-cis-diltiazem (Fig. 7e). Indeed, VGCC block with diltiazem was recently shown to activate SOCE in vascular smooth muscle cells [51] and this process is likely to selectively activate calpain-2 [52]. Thus, in photoreceptors, a degeneration that is initially caused by very low Ca^{2+} levels

may be linked to an excessive increase of Ca^{2+} and calpain-2 activity via SOCE, perhaps explaining the apparent contradiction between the high and low Ca^{2+} hypothesis for neurodegeneration.

In *rd1* retina, the loss of PDE6 activity and the concomitant rise in cGMP levels causes CNGC over-activation, strong photoreceptor depolarization, and likely a constant opening of VGCCs (Fig. 7f). The elevation of CNGC activity will also trigger over-activation of NCKX and NKX and thus *rd1* rods may be experiencing ATP depletion, something which then would stop PMCA-mediated Ca^{2+} extrusion in cell body and synapse. This would lead to an uncontrolled rise in intracellular Ca^{2+} levels and is in line with the observed activation of calpain-type proteases in photoreceptor cell body and synapse.

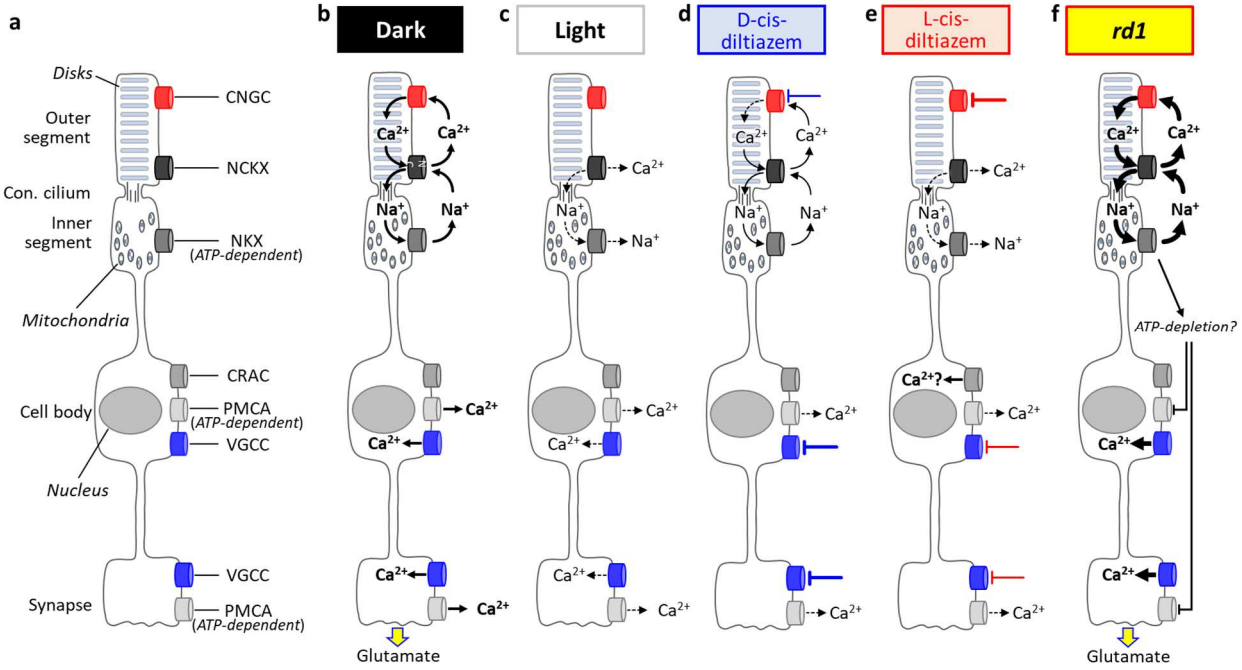

Fig. 7: Schematic representation of photoreceptor Ca^{2+} flux under different experimental conditions. (**a**) The phototransduction cascade is compartmentalized to the photoreceptor outer segments, which harbour cyclic nucleotide-gated channel (CNGC) and $Na^+/Ca^{2+}/K^+$ exchanger (NCKX). The connecting cilium links outer to inner segment, which holds almost all mitochondria and the ATP-driven Na^+/K^+ exchanger (NKX). The cell body harbours the nucleus as well as Ca^{2+}-release activated channel (CRAC), plasma membrane Ca^{2+}-ATPase (PMCA), and voltage-gated Ca^{2+} channels VGCC. PMCA and VGCC are also found in the synapse. (**b**) In the dark there is a continuous flux of Ca^{2+} ions entering the outer segment via CNGC and exiting via NCKX. The Na^+ gradient needed to drive NCKX is maintained by the ATP-dependent NKX in the inner segment. The flux of Na^+ and Ca^{2+} ions across the photoreceptor membrane (*i.e.* the dark current) keeps the cell in a continuously depolarized state. At the same time, in the photoreceptor cell body and synapse, VGCC allows for Ca^{2+} influx, mediating synaptic glutamate release. In the cell body and synapse Ca^{2+} is extruded by the ATP-

dependent PMCA. (**c**) In light CNGC closes, while Ca^{2+} continues to exit the cell via NCKX, leading to photoreceptor hyperpolarization. This in turn closes VGCC, ending synaptic glutamate release. (**d**) D-cis-diltiazem (blue lines) inhibits predominantly VGCC, with a partial block on CNGC at high concentrations. (**e**) L-cis-diltiazem (red lines) blocks predominantly CNGC, with an additional block on VGCC at high concentrations. This resembles a situation of "constant light" and may cause a depletion of intracellular Ca^{2+} and secondary Ca^{2+} influx via activation of CRAC. (**f**) In *rd1* photoreceptors high cGMP continuously opens CNGC, representing a situation of "constant darkness". Possibly, excessive NKX activity in *rd1* causes a depletion of ATP, preventing Ca^{2+} extrusion via PMCA.

Can diltiazem restore Ca^{2+} homeostasis in photoreceptors?

In rod photoreceptor diseases like RP, where a treatment may aim to prevent excessive Ca^{2+} influx into the rod OS, while still preserving cone functionality, a strong rod over cone selectivity is highly desirable. In the present study, we found the CNGC blocker L-cis-diltiazem to have this desired trait, to show a reasonably good rod *vs*. cone selectivity. However, we were unable to demonstrate a protective effect of L-cis-diltiazem on *rd1* retina – even though L-cis-diltiazem was highly effective on heterologously-expressed rod CNGC, and these channels were expressed in *rd1* photoreceptors during the treatment period. Even worse, at higher concentrations, L-cis-diltiazem showed obvious signs of toxicity, in wt, *rd1*, and *rd10* retina. Thus, the effects of pharmacological inhibition with L-cis-diltiazem appear to be different from the effects of genetic inactivation of CNGC in *rd1* * *Cngb1*$^{-/-}$ double-mutant mouse [12]. Then again, loss-of-function mutations in CNGC genes cause photoreceptor degeneration in both RP [53] and ACHM [54]. Hence, on a genetic level, low activity of CNGC and decreased Ca^{2+} influx into photoreceptor outer segments is clearly connected to photoreceptor degeneration.

An explanation for the discrepant results on genetic and pharmacological CNGC inactivation in *rd1* retina could be the assembly of CNGA1 homotetrameric channels in the absence of the CNGB1a subunit [55]. While rod photoreceptors may fail to efficiently target homomeric CNGA1 channels to the outer segment plasma membrane [56], in the *rd1* * *Cngb1*$^{-/-}$ double-mutant situation, homomeric CNGA1 channels may still allow for a low level of Ca^{2+} influx into the photoreceptor, with baseline activity of VGCC enabling additional Ca^{2+} influx. In contrast, in our experiments, at high doses of L-cis-diltiazem, Ca^{2+} influx via CNGC was strongly inhibited, likely resulting in cell death due to depletion of intracellular Ca^{2+} stores and activation of SOCE (see above). Independent of SOCE, low photoreceptor Ca^{2+} levels will result in disinhibition of guanylyl cyclase and

exceedingly high cGMP production, which may then kill photoreceptors via over-activation of cGMP-dependent protein kinase G (PKG) [5, 57].

Incidentally, inhibition of VGCC with D-cis-diltiazem in our hands also failed to show significant photoreceptor protection. This is in line with a number of earlier studies (reviewed in [20]) and corroborates on a pharmacological level our previous study employing the *rd1* * *Cacna1f*$^{-/-}$ double-mutant mouse, *i.e.* an *rd1* mouse in which the synaptic VGCC was dysfunctional [19]. In contrast to L-cis-diltiazem, D-cis-diltiazem did not appear to be overly retinotoxic even at high concentrations. This may correspond to the genetic situation where loss-of-function mutations in VGCC impair synaptic transmission from photoreceptors to second order neurons. In humans such mutations can cause night-blindness, but do not usually cause photoreceptor degeneration [58]. However, activity of VGCC seems relevant for mediating calpain activation in photoreceptors.

Calpain activity, Ca^{2+}, and cell death

Previously, we had proposed that calpain activation in dying photoreceptors was mediated by CNGC, triggered by high intracellular cGMP-levels [37]. Considering our current data, this simple chain of causality may be incorrect. The activity of calpain that we observed appeared to be localized predominantly to the photoreceptor cell body and the synaptic region. In fact, calpain activity was conspicuously absent from the OS where the highest CNGC-dependent Ca^{2+} influx would be expected. The low mobility of Ca^{2+} ions from OS to the rest of the photoreceptor cell [16, 59, 60] argues against the possibility of Ca^{2+} flowing into the OS via CNGC and activating calpain in the cell body and beyond. However, calpain activation could be mediated indirectly by voltage-dependent Ca^{2+} influx via VGCC expressed in cell body and synapse. This would be in line with our previous study, where genetic inactivation of VGCC strongly reduced calpain activity in *rd1* photoreceptors [19]. Hence, the chain of causality leading from high cGMP to calpain activation is likely to include VGCC mediated Ca^{2+} influx.

In addition, we found that the ratio between dying and calpain positive cells was strongly reduced by treatment with either of the two diltiazem enantiomers, notably, without an overall reduction of cell death. This suggests that calpain activity found in disease models may be a secondary event, *i.e.* a process that contributes to the degeneration of photoreceptors but that is by itself not a significant cause of cell death.

721 Excessive Ca^{2+} influx via CNGC and/or VGCC has for a long time been suggested as
722 a major driver for photoreceptor cell death [12, 46]. However, follow-up studies have
723 produced contradictory results, raising the question as to whether CNGC, VGCC, or Ca^{2+}
724 as such, really are disease drivers [20]. Our present study sheds light onto this enigma
725 and demonstrates that both D- and L-cis enantiomers of the anti-hypertensive drug
726 diltiazem can reduce photoreceptor Ca^{2+} influx. Remarkably, treatment with either
727 compound and inhibition of either VGCC or CNGC did not result in photoreceptor
728 protection. Moreover, the use of L-cis-diltiazem and the concomitant reduction of Ca^{2+}
729 influx had strong detrimental effects on photoreceptor viability, indicating that Ca^{2+}-influx
730 was in fact protective, rather than destructive. Taken together, this suggests the so-called
731 "low Ca^{2+}" hypothesis as the more likely explanation for photoreceptor degeneration [47].
732 These findings are highly relevant for therapy development as they shift the focus from
733 Ca^{2+}-dependent to cGMP-dependent degenerative mechanisms.

IV. METHODS

Animals

Mice used for experiments were bred and handled according to the German law on animal protection. The experimental procedures involving animals were reviewed and approved by the institutional animal welfare committee of the University of Tübingen. Animals were maintained in the Tübingen Institute for Ophthalmic Research specified-pathogen-free (SPF) housing facility, under 12h/12h light/dark cycle, had *ad libitum* access to food and water, and were used irrespective of gender.

For retinal explant cultures C3H/HeA *Pde6b* $^{rd1/rd1}$ animals (*rd1*) and their respective congenic wild-type C3H/HeA *Pde6b* $^{+/+}$ counterparts (*wt*) were used [61]. Further studies were performed on explants derived from C57BL/6J $^{rd10/rd10}$ animals (*rd10*) [37]. For studying light-induced Ca^{2+} responses in cone photoreceptors, we used transgenic mice expressing the Ca^{2+} biosensor TN-XL [62] under the human red opsin promoter HR2.1 on a C57BL/6j background [16].The procedures regarding the *Xenopus laevis* frogs and the handling of the oocytes had approval from the authorized animal ethics committee of the Friedrich Schiller University Jena, Germany. The respective protocols were performed in accordance with the approved guidelines.

Molecular biology and functional expression of heterotetrameric CNGCs in *Xenopus laevis* oocytes

The coding sequences for the retinal CNGC subunits, bovine CNGA1 (NM_174278.2) [41] and CNGB1a (NM_181019.2) [63] from rod photoreceptors and human CNGA3 (NM_001298.2) [64] and CNGB3 [65] from cone photoreceptors, were subcloned into the pGEMHE vector [66] for heterologous expression in *Xenopus laevis* oocytes. The cDNA encoding for the human cone CNGB3 subunit was kindly provided by M. Varnum (Washington State University, USA) and for the bovine CNGB1a subunit by W. Zagotta (University of Washington, USA). The surgical removal of oocytes was performed from adult frog females under anaesthesia (0.3% tricaine; MS-222, Pharmaq Ltd., Fordingbridge, UK). The oocytes were treated with collagenase A (3 mg/ml; Roche) for 105 min in Barth's solution containing (in mM) 82.5 NaCl, 2 KCl, 1 $MgCl_2$, and 5 HEPES, pH 7.5. After this procedure, oocytes of stages IV and V were manually dissected and injected with the genetic material encoding for the CNGC from rod and cone photoreceptors. For efficient generation of heterotetrameric channels, the ratio of CNGA3 mRNA to CNGB3 mRNA was 1:2.5 [26] and of CNGA1 mRNA to CNGB1a mRNA was 1:4 [67]. After injection, the oocytes were kept at 18°C for 2 to 7 days in Barth's solution

containing (in mM) 84 NaCl, 1 KCl, 2.4 $NaHCO_3$, 0.82 $MgSO_4$, 0.41 $CaCl_2$, 0.33 $Ca(NO_3)_2$, 7.5 Tris, cefuroxime (4.0 $\mu g \times ml^{-1}$), and penicillin/streptomycin (100 $\mu g \times ml^{-1}$), pH 7.4.

Electrophysiology

Macroscopic ionic currents were measured with the patch-clamp technique and the inside-out configuration, using an Axopatch 200B patch-clamp amplifier (Axon Instruments, Foster City, CA). Recordings were made at room temperature. Current data were acquired using PATCHMASTER software (HEKA Elektronik, Lambrecht, Germany) with a sampling frequency of 5 kHz, and low-pass filtered at 2 kHz. From a holding potential of 0 mV, currents were elicited by voltage steps to -65 mV, then to -35 mV, and back to 0 mV. When mentioned, also voltage steps to -100 mV and +100 mV were recorded. The patch pipettes were pulled from borosilicate glass tubing (outer diameter 2.0 mm, inner diameter 1.0 mm; Hilgenberg GmbH, Germany). The initial resistance was 0.6-1.3 MΩ. Intracellular and extracellular solutions contained 140 mM NaCl, 5 mM KCl, 1 mM EGTA, and 10 mM HEPES (pH 7.4). The solutions used for the Ca^{2+}-containing recordings were: 120 mM NaCl, 3 mM KCl, 2 mM NTA, 0.5 mM niflumic acid, 10 mM HEPES and 1 mM $CaCl_2$ (pH 7.4) for the extracellular side and 145 mM KCl, 8 mM NaCl, 2 mM NTA, 10 mM HEPES and 0.05 mM $CaCl_2$ (pH 7.4) for the intracellular side [30].

The cyclic nucleotides, cAMP (Merck KGaA, Darmstadt, Germany) or cGMP (Biolog LSI GmbH & Co KG, Bremen, Germany), were added to intracellular solutions as indicated. Either D- or L-cis-diltiazem (Abcam - ab120260 and Abcam - ab120532, respectively, Germany) were added to the cGMP-containing solutions to a final concentration of 25 µM and 100 µM as required. The diltiazem-containing solutions were prepared from stock solutions (10 mM) immediately before the experiments. The cGMP-solutions, or solution mixtures containing cGMP and either D- or L-cis-diltiazem were administered via a multi-barrel application system to the cytosolic face of the patch.

For studying channel's activation and deactivation kinetics in the presence of D- or L-cis-diltiazem we performed fast jumps of the ligand concentration (from zero to either 3 mM cGMP or 3 mM cGMP + 100 µM D- or L-cis-diltiazem and back to zero) by means of a double-barrelled θ-glass pipette mounted on a piezo-driven device [68]. The recording rate was 20 Hz. The solution exchange at the pipette tip was completed within 1 ms [69].

Confocal patch-clamp fluorometry (cPCF)

The influence of D- and L-cis-diltiazem on cGMP binding was studied by means of confocal patch-clamp fluorometry (cPCF). The method has been described in detail previously [33, 70, 71]. The experiments for measuring ligand binding and channel gating simultaneously were performed in inside-out macropatches of *X. laevis* oocytes expressing heterotetrameric rod CNGC, at -35 mV. As fluorescent ligand we used 8-[DY-547]-AHT-cGMP (f*cGMP). 8-[DY-547]-AHT-cGMP was prepared in analogy to the related cyclic nucleotides 8-[DY-547]-AET-cGMP and 8-[DY-547]-AHT-cAMP [33, 35]. To be able to differentiate between the fluorescence of the bound f*cGMP from the fluorescence generated by the free f*cGMP in the bath solution, we used an additional red dye, DY647 (Dyomics, Jena, Germany), at a concentration of 1 µM. Recordings were performed with an LSM 710 confocal microscope (Carl Zeiss Jena GmbH, Germany) and were triggered by the ISO3 hard- and software (MFK, Niedernhausen, Germany; sampling rate 5 kHz, 4-pole Bessel filter set to 2 kHz). Due to the relative long duration of the experiment, to avoid cell-membrane exposure to damaging amounts of light, binding was measured under steady-state conditions, during pre-selected time windows only: in the presence of 10 µM f*cGMP, during the jump to 10 µM f*cGMP + 100 µM L-cis-diltiazem and several times during L-cis-diltiazem removal from the open channels.

Colocalization experiments

To verify the correct incorporation of heterotetrameric CNGCs into the oocyte plasma membrane we labelled the cone CNGB3- and rod CNGB1a-subunit by fusing enhanced GFP to their intracellularly located C terminus. At first, we introduced an *Avr*II site in pGEMHE-CNGB1a by site-directed mutagenesis at CNGB1a K1205 which was thereby changed to R1205. Afterwards, the PCR amplified *EGFP* gene was ligated into the newly generated *Avr*II site of the pGEHME-CNGB1a construct. To fuse EGFP into CNGB3 C-terminus, we introduced an *Xho*I site in pGEMHE-CNGB3 by site-directed mutagenesis at CNGB3 P668 and K669 which were thereby changed to leucine (L668) or glutamate (E669), respectively. Afterwards, the PCR amplified *EGFP* gene was ligated into the newly generated *Xho*I site of the pGEHME-CNGB3 construct. The correct insertion of PCR products was confirmed by DNA sequencing.

The oocyte membrane was stained from the extracellular side with fluorescently labelled lectin (Alexa Fluor™ 633 - wheat germ agglutinin (Alexa-WGA), Invitrogen Life Technologies Corporation, Eugene, Oregon, red fluorescence signal). For this the oocytes were incubated in 5 µg/ml Alexa-WGA for 7 minutes. Alexa-WGA was excited with the 633-nm line of a helium neon laser. GFP was excited with the 488-nm line of an

argon laser. Fluorescence signals, measured along an imaginary line perpendicular to the plasma membrane, were quantified by confocal microscopy (LSM 710, Carl Zeiss Jena GmbH, Jena, Germany). The GFP- and WGA-fluorescence profiles were constructed using the LSM 710 image analysis software.

Analysis of the oocyte data

For concentration-activations relationships, each patch was first exposed to a solution containing no cGMP and then to a solution containing the saturating concentration of 3 mM cGMP. After subtracting the baseline current from the current amplitude in the presence of cGMP, the current response for each ligand concentration was normalized to the saturating current. The experimental data points were fitted using the Hill equation:

$$\frac{I}{I_{max}} = \frac{1}{1+\left(\frac{EC_{50}}{x}\right)^{H}} \quad \text{(Equation 1)}$$

where I is the current amplitude, I_{max} is the maximum current induced by a saturating cGMP concentration, x is the ligand concentration, EC_{50} is the ligand concentration of half maximum effect, and H is the Hill coefficient. The analysis was performed with OriginPro 2016G software (OriginLab Corporation, Northampton, USA). Experimental data are given as mean ±SEM.

The effect of either D- or L-cis- diltiazem was quantified by measuring the cGMP-induced current, under steady-state conditions at the end of either -100 mV, -35 mV, or +100 mV pulse, in the presence of diltiazem as required. The amount of diltiazem block (%) is related to the current at the respective cGMP concentration and the amount of current decrease in the presence of diltiazem and was calculated as follow (here exemplified for the 100 µM cGMP-induced current):

$$diltiazem\ block\ (\%) = 100 - \frac{\frac{I(100\mu M\ cGMP + x\ \mu M\ Diltiazem)}{I(3mM\ cGMP + x\ \mu M\ Diltiazem)} \cdot 100}{\frac{I(100\mu M\ cGMP)}{I(3mM\ cGMP)}}$$

(Equation 2)

The time courses for channel activation, deactivation (starting after the respective initial delay due to diltiazem removal) and diltiazem block were fitted with a single exponential:

$$I(t) = A * exp\left[\frac{-t}{\tau}\right] \quad \text{(Equation 3)}$$

where A is the amplitude, t the time, and τ the time constant for either activation, deactivation, or block.

The time course for diltiazem washout was fitted with a double exponential function:

$$I(t) = A_1 * exp\left[\frac{-t}{\tau_{fast}}\right] + A_2 * exp\left[\frac{-t}{\tau_{slow}}\right] + y_0 \quad \text{(Equation 4)}$$

where A_1,A_2 are the amplitudes of the fast and slow components, t the time, and τ_{fast} and τ_{slow} the time constants for the fast and slow phase of the diltiazem washout.

For the statistical analysis of D- and L-cis-diltiazem effect on retinal CNGCs, we used the two-tailed unpaired Student *t*-test. Figures were prepared using CorelDraw X7 (Corel, Ottawa, Canada)

Retinal explant culture

To assess the effects of D- and L-cis-diltiazem on calpain activity and photoreceptor degeneration, *rd1* retinas were explanted at post-natal day (P5), while retinas from more slowly degenerating *rd10* animals were explanted at P9. The explants were cultured on a polycarbonate membrane (Corning-Costar Transwell permeable support, 24 mm insert, #CLS3412) with complete medium (Gibco R16 medium with supplements) [72]. The R16 medium was exchanged every two days with treatment added at either P7 and P9, for *rd1*, or at P11, P13, P15 for *rd10* explants. The cultures were treated with 25, 50, and 100 µM of D- and L-cis-diltiazem, respectively. Cultures were ended on P11 (*rd1*) and P17 (*rd10*) by fixing the cultures with 4% paraformaldehyde (PFA). The explants were embedded in Tissuetek (Sakura Finetek Europe B.V.) and sectioned (12 µm) in a cryostat (ThermoFisher Scientific, CryoStar NX50 OVP, Runcorn UK).

TUNEL staining

The TUNEL (terminal deoxynucleotidyl transferase dUTP nick end labelling) assay kit (Roche Diagnostics, Mannheim, Germany) was used to label dying cells. Histological sections from retinal explants were dried and stored at -20°C. The sections were rehydrated with phosphate-buffered saline (PBS; 0.1M) and incubated with Proteinase K (1.5 µg/µl) diluted in 50 mM TRIS-buffered saline (TBS; 1 µl enzyme in 7 ml TBS) for 5 mins. This was followed by 3 times 5 minutes TBS washing and incubation with a mixture of 30% HCl and 70% ethanol for 5 min to increase the accessibility of cells to the enzyme. Another 3 times 5 minutes washing was followed by incubation with blocking solution (10% normal goat serum, 1% bovine serum albumin, 1% fish gelatine in phosphate-buffered saline with 0.03% Tween-20). TUNEL staining solution was prepared using 10 parts of blocking solution, 9 parts of TUNEL labelling solution and 1 part of TUNEL enzyme. After blocking, the sections were incubated with TUNEL staining solution

overnight at 4° C. Finally, the sections were washed 2 times with PBS, mounted using Vectashield with DAPI (Vector Laboratories Inc, Burlingame, CA, USA) and imaged under a Zeiss (ApoTome.2) microscope for further analysis.

Calpain-activity assay

This assay allows resolving overall calpain activity *in situ*, on unfixed tissue sections [14]. Retinal tissue sections were incubated and rehydrated for 15 minutes in calpain reaction buffer (CRB) (5.96 g HEPES, 4.85 g KCl, 0.47 g $MgCl_2$, 0.22 g $CaCl_2$ in 100 ml ddH_2O; pH 7.2) with 2 mM dithiothreitol (DTT). The tissue sections were incubated for 2 hours at 37°C in CRB with tBOC-Leu-Met-CMAC (5 µM; Thermofisher Scientific, A6520). Afterwards, the tissue sections were washed twice in PBS (5 minutes) and mounted using Vectashield mounting medium (Vector) for immediate visualization under the ZEISS ApoTome2.

Immunohistochemistry

The cryo-sectioned slides were dried for 30 minutes at 37ºC and hydrated for 15 minutes. The sections were then incubated with blocking solution (10% NGS, 1% BSA and 0.3% PBST) for one hour. The primary antibodies CNGB1 (Sigma-Aldrich, HPA039159; 1:1000), calpain-2 (Abcam, ab39165; 1:300), or caspase-3 (Cell Signalling, 9664; 1:1000) were diluted in blocking solution and incubated overnight at 4ºC. Rinsing with PBS for 3 times 10 minutes each was followed by incubation with secondary antibody (Molecular Probes, AlexaFluor488 (A01134) or AlexaFluor562 (A11036), diluted 1:500 in PBS) for one hour. The sections were further rinsed with PBS for 3 times 10 minutes each and mounted with Vectashield containing DAPI (Vector).

Microscopy and image analysis in retinal cultures

The images of *ex vivo* retina and organotypic explant cultures were captured using a Zeiss Imager Z.2 fluorescence microscope, equipped with ApoTome2, an Axiocam 506 mono camera, and HXP-120V fluorescent lamp (Carl Zeiss Microscopy, Oberkochen, Germany). The excitation ($\lambda_{Exc.}$) / emission ($\lambda_{Em.}$) characteristics of the filter sets used for the different fluorophores were as follows (in nm): DAPI ($\lambda_{Exc.} = 369\,nm,\ \lambda_{Em.} = 465\,nm$), AF488 ($\lambda_{Exc.} = 490\,nm,\ \lambda_{Em.} = 525\,nm$), and AF562 ($\lambda_{Exc.} = 578\,nm,\ \lambda_{Em.} = 603\,nm$). The Zen 2.3 blue edition software (Zeiss) was used to capture images (both tiled and z-stack, 20x magnification). The data were collected from 7-9 different sections obtained from 3-5 animals. Sections of 12 µm thickness were analysed using 8-12

928 Apotome Z-planes. The positive cells in the ONL were manually quantified, the ONL area
929 was measured in Zen 2.3 software. The total number of cells in the ONL was calculated
930 using an average cell (nucleus) size and the percent positive cells was determined with
931 respect to the total number of cells in the same ONL area. Values were normalized to
932 control condition (100%).

933 The relative localization of positive cells within the ONL was assessed by dividing the
934 width of the ONL horizontally into two equal halves (*i.e.* upper and lower half) and
935 manually quantifying the distribution of positive cells in each of the halves. The chance
936 level for cell distribution was 50%. The percent of degenerating photoreceptors localized
937 close to OPL, were analysed by comparing cell count in the lower half of ONL to total
938 positive cells in the ONL.

939

940 **Statistical analysis for retinal cultures**

941 Linear mixed-effects models were fitted by restricted maximum likelihood estimation
942 (REML), to assess the significance of the effects in explaining the variations of the
943 dependent variables. Variance inflation factors (VIF) of the predictor variables were
944 calculated and assured to fall well below the common threshold value, indicating no
945 collinearity between them [73]. The residuals were confirmed visually to follow a normal
946 distribution, while homoscedasticity (homogeneity of the residual variances) was tested
947 using the Brown–Forsythe test [74] and reported in case of violations.

948 Figures were prepared using Photoshop CS5 (Adobe, San Jose, CA, USA). Statistical
949 analysis and graph preparation were performed using JMP 15.2.0 (466311, SAS Institute
950 Inc, Cary, NC, USA).

951 **Two-photon Ca^{2+} imaging**

952 Light stimulus-evoked Ca^{2+} responses were recorded in cone axon terminals using a
953 two-photon (2P) microscope, as previously described [75]. In brief, we used adult (~ P90)
954 transgenic HR2.1:TN-XL mice (for details, see above). After two hours of dark adaptation
955 [16], the animal was deeply anesthetized with isoflurane (CP-Pharma, Germany), and
956 then sacrificed by cervical dislocation. All procedures were performed under dim red
957 illumination. Following enucleation of the eyes, the retinas were dissected and vertically
958 sliced (~200 µm) in artificial cerebral spinal fluid (ACSF), which contained (in mM): 125
959 NaCl, 2.5 KCl, 2 $CaCl_2$, 1 $MgCl_2$, 1.25 NaH_2PO_4, 26 $NaHCO_3$, 0.5 L-glutamine, and 20
960 glucose (Sigma-Aldrich or Merck, Germany) and was maintained at pH 7.4 with

carboxygen (95% O_2, 5% CO_2). Next, the slices were transferred to the 2P microscope's recording chamber and superfused with warmed (37°C) ACSF.

The 2P microscope, a customized MOM (Sutter Instruments, Novato, USA; [76], was driven by a mode-locked Ti:Sapphire laser (MaiTai-HP DeepSee; Newport Spectra-Physics, Darmstadt, Germany) tuned to 860 nm. For further technical details on the 2P setup configuration, see [75]. TN-XL is a ratiometric FRET-based Ca^{2+} indicator [62], therefore we used two detection channels with the appropriate band-pass (BP) filters (483 BP 32; 535 BP 50; AHF, Tübingen, Germany) to capture both the sensor's donor (F_D; ECFP) and acceptor fluorescence (F_A; citrine) simultaneously. The relative Ca^{2+} level in the cone terminals was then represented by the ratio F_A/F_D (*cf.* Fig. 4b,c). Light stimuli were presented using a custom-built stimulator [77] with two band-pass filtered LEDs (UV filter: 360 BP 12; green: 578 BP 10; AHF) mounted below the recording chamber.

Before presenting light flashes and recording cone Ca^{2+} signals, slices were adapted to a constant background illumination equivalent to a photoisomerisation rate of ~10^4 P*/cone s^{-1} for ≥ 15 seconds. Light stimuli consisted of a series of 1-s bright flashes at 0.25 Hz, evoking similar photoisomerisation rates (~$6.5 \cdot 10^3$ P*s^{-1}/cone) in both mouse cone types.

Stock solutions (100mM) of D- and L-cis-diltiazem were prepared in distilled water and stored at 4°C. Prior to each experiment, D- or L-cis-diltiazem dilutions were freshly prepared from the stock in carboxygenated ACSF solution. For bath application, the tissue was perfused with D- or L-cis-diltiazem (25, 50, or 100 µM) added to the bathing solution for ≥ 1 minute before commencing the recording; the perfusion rate was of ~1.5 ml/minute. Drug entry into the recording chamber was confirmed by adding Sulforhodamine 101 (Sigma-Aldrich) to the drug solution.

Analysis of Ca^{2+} imaging data

To identify the factors (*i.e.* L-cis *vs.* D-cis, concentration) that are significant for predicting the response of a cell during drug treatment (a potential change in AUC), we applied a multivariate linear model [78]. The importance of each factor was estimated as its impact on the predictive power of the statistical model (*cf.* Fig. 4d). The effect of each factor was considered both individually and in interactions with the other variables, to identify which factor or group of factors is best at modelling the AUC values. The explanatory variables were standardised prior to model fitting, by subtracting the mean and dividing by the standard deviation of the variable. As before, the statistical

assumptions of the linear model were evaluated. The VIF for each explanatory variable was found to fall below the common threshold, indicating a lower level of multicollinearity. Visual inspection showed that the residuals were approximately normally distributed. A Brown-Forsythe test indicated that there was heteroscedasticity in the data, though as previously noted these models are robust to such variability. The model also incorporated a random effects term for the recording field, which controlled for recordings where the ROIs were on average higher or lower than the mean across all ROIs in all recordings. Specifically, the modelling showed that (1) more active cells (higher AUC) were more sensitive to the drug application, (2) there was a statistically significant difference between the effects of L- and D-cis- diltiazem on the AUC, and (3) the drug concentration also had a significant effect on AUC.

The effect size is determined using the method for estimating semi-partial R-squared [78] and allowed us to compare the relative impact of each factor in the linear mixed effects model (Supplemental Table 3). This method also allowed us to evaluate the fit for the whole model (SPRS = 0.368).

REFERENCES

1. Kennan, A., A. Aherne, and P. Humphries, *Light in retinitis pigmentosa.* Trends Genet, 2005. **21**(2): p. 103-110.
2. Narayan, D.S., et al., *A review of the mechanisms of cone degeneration in retinitis pigmentosa.* Acta Ophthalmol, 2016. **94**(8): p. 748-754.
3. Hamel, C.P., *Cone rod dystrophies.* Orphanet Journal of Rare Diseases, 2007. **2**(1): p. 7.
4. Paquet-Durand, F., V. Marigo, and P. Ekström, *RD Genes Associated with High Photoreceptor cGMP-Levels (Mini-Review).* Adv Exp Med Biol, 2019. **1185**: p. 245-249.
5. Power, M., et al., *Cellular mechanisms of hereditary photoreceptor degeneration - Focus on cGMP.* Prog Retin Eye Res, 2020. **74**: p. 100772.
6. Kaupp, U.B. and R. Seifert, *Cyclic nucleotide-gated ion channels.* Physiol Rev, 2002. **82**(3): p. 769-824.
7. Wetzel, R.K., E. Arystarkhova, and K.J. Sweadner, *Cellular and Subcellular Specification of Na,K-ATPase α and β Isoforms in the Postnatal Development of Mouse Retina.* The Journal of Neuroscience, 1999. **19**(22): p. 9878-9889.
8. Ames, A. and Y.Y. Li, *Energy requirements of glutamatergic pathways in rabbit retina.* The Journal of Neuroscience, 1992. **12**(11): p. 4234.
9. Ingram, N.T., A.P. Sampath, and G.L. Fain, *Membrane conductances of mouse cone photoreceptors.* J Gen Physiol, 2020. **152**(3).
10. Waldner, D.M., N.T. Bech-Hansen, and W.K. Stell, *Channeling Vision: Ca(V)1.4-A Critical Link in Retinal Signal Transmission.* Biomed Res Int, 2018. **2018**: p. 7272630.
11. Wegierski, T. and J. Kuznicki, *Neuronal calcium signaling via store-operated channels in health and disease.* Cell Calcium, 2018. **74**: p. 102-111.
12. Paquet-Durand, F., et al., *A key role for cyclic nucleotide gated (CNG) channels in cGMP-related retinitis pigmentosa.* Hum Mol Genet, 2011. **20**(5): p. 941-7.
13. Fox, D.A., A.T. Poblenz, and L.H. He, *Calcium overload triggers rod photoreceptor apoptotic cell death in chemical-induced and inherited retinal degenerations.* Oxidative/Energy Metabolism in Neurodegenerative Disorders, 1999. **893**: p. 282-285.
14. Vallazza-Deschamps, G., et al., *Excessive activation of cyclic nucleotide-gated channels contributes to neuronal degeneration of photoreceptors.* Eur J Neurosci, 2005. **22**(5): p. 1013-22.
15. Bowes, C., et al., *Localization of a retroviral element within the rd gene coding for the beta subunit of cGMP phosphodiesterase.* Proc Natl Acad Sci U S A, 1993. **90**(7): p. 2955-9.

16. Wei, T., et al., *Light-driven calcium signals in mouse cone photoreceptors.* J Neurosci, 2012. **32**(20): p. 6981-94.

17. Kulkarni, M., et al., *Calcium dynamics change in degenerating cone photoreceptors.* Hum Mol. Genet, 2016.

18. Wang, T., et al., *The PDE6 mutation in the rd10 retinal degeneration mouse model causes protein mislocalization and instability and promotes cell death through increased ion influx.* J Biol Chem, 2018. **293**(40): p. 15332-15346.

19. Schon, C., F. Paquet-Durand, and S. Michalakis, *Cav1.4 L-Type Calcium Channels Contribute to Calpain Activation in Degenerating Photoreceptors of rd1 Mice.* PLoS One, 2016. **11**(6): p. e0156974.

20. Barabas, P., P.C. Cutler, and D. Krizaj, *Do calcium channel blockers rescue dying photoreceptors in the Pde6b (rd1) mouse?* Adv. Exp. Med. Biol, 2010. **664**: p. 491-499.

21. Hart, J., et al., *Inhibitory action of diltiazem on voltage-gated calcium channels in cone photoreceptors.* Exp Eye Res, 2003. **76**(5): p. 597-604.

22. Stern, J.H., U.B. Kaupp, and P.R. MacLeish, *Control of the light-regulated current in rod photoreceptors by cyclic GMP, calcium, and l-cis-diltiazem.* Proc Natl Acad Sci U S A, 1986. **83**(4): p. 1163-7.

23. Haynes, L.W., *Block of the cyclic GMP-gated channel of vertebrate rod and cone photoreceptors by l-cis-diltiazem.* J Gen Physiol, 1992. **100**(5): p. 783-801.

24. Cia, D., et al., *Voltage-gated channels and calcium homeostasis in mammalian rod photoreceptors.* J Neurophysiol, 2005. **93**(3): p. 1468-75.

25. Shuart, N.G., et al., *Molecular mechanism for 3:1 subunit stoichiometry of rod cyclic nucleotide-gated ion channels.* Nat Commun, 2011. **2**: p. 457.

26. Peng, C., E.D. Rich, and M.D. Varnum, *Subunit configuration of heteromeric cone cyclic nucleotide-gated channels.* Neuron, 2004. **42**(3): p. 401-10.

27. Pugh, E.N. and T.D. Lamb, *Phototransduction in vertebrate rods and cones: Molecular mechanism of amplification, recovery and light adaptation*, in *Molecular Mechanisms in Visual Transduction*, D.G. Stavenga, W.J. DeGrip, and E.N. Pugh Jr, Editors. 2000, Elsevier B.V. p. 581.

28. Cote, R.H. and M.A. Brunnock, *Intracellular cGMP concentration in rod photoreceptors is regulated by binding to high and moderate affinity cGMP binding sites.* J Biol Chem, 1993. **268**(23): p. 17190-8.

29. Nakatani, K. and K.W. Yau, *Calcium and light adaptation in retinal rods and cones.* Nature, 1988. **334**(6177): p. 69-71.

30. Frings, S., et al., *Profoundly different calcium permeation and blockage determine the specific function of distinct cyclic nucleotide-gated channels.* Neuron, 1995. **15**(1): p. 169-79.

31. Picones, A. and J.I. Korenbrot, *Permeability and interaction of Ca2+ with cGMP-gated ion channels differ in retinal rod and cone photoreceptors.* Biophysical Journal, 1995. **69**(1): p. 120-127.

32. Nache, V., et al., *Hysteresis of ligand binding in CNGA2 ion channels.* Nat Commun, 2013. **4**: p. 2866.

33. Biskup, C., et al., *Relating ligand binding to activation gating in CNGA2 channels.* Nature, 2007. **446**(7134): p. 440-443.

34. Zheng, J. and W.N. Zagotta, *Gating rearrangements in cyclic nucleotide-gated channels revealed by patch-clamp fluorometry.* Neuron, 2000. **28**(2): p. 369-74.

35. Nache, V., et al., *Deciphering the function of the CNGB1b subunit in olfactory CNG channels.* Sci Rep, 2016. **6**: p. 29378.

36. Schielzeth, H., et al., *Robustness of linear mixed-effects models to violations of distributional assumptions.* Methods in Ecology and Evolution, 2020. **11**(9): p. 1141-1152.

37. Arango-Gonzalez, B., et al., *Identification of a common non-apoptotic cell death mechanism in hereditary retinal degeneration.* PLoS One, 2014. **9**(11): p. e112142.

38. Power, M.J., et al., *Systematic spatiotemporal mapping reveals divergent cell death pathways in three mouse models of hereditary retinal degeneration.* J Comp Neurol, 2020. **528**(7): p. 1113-1139.

39. Nicholson, D.W., et al., *Identification and inhibition of the ICE/CED-3 protease necessary for mammalian apoptosis.* Nature, 1995. **376**(6535): p. 37-43.

40. Vighi, E., et al., *Combination of cGMP analogue and drug delivery system provides functional protection in hereditary retinal degeneration.* Proc Natl Acad Sci U S A, 2018. **115**(13): p. E2997-e3006.

41. Kaupp, U.B., et al., *Primary structure and functional expression from complementary DNA of the rod photoreceptor cyclic GMP-gated channel.* Nature, 1989. **342**(6251): p. 762-6.

42. Bocchero, U., et al., *Electrophysiological Changes During Early Steps of Retinitis Pigmentosa.* Invest Ophthalmol Vis Sci, 2019. **60**(4): p. 933-943.

43. McLatchie, L.M. and H.R. Matthews, *Voltage-dependent block by L-cis-diltiazem of the cyclic GMP-activated conductance of salamander rods.* Proc Biol Sci, 1992. **247**(1319): p. 113-9.

44. Tang, L., et al., *Structural Basis for Diltiazem Block of a Voltage-gated Ca2+ Channel.* Mol Pharmacol, 2019.

45. Zhao, Y., et al., *Molecular Basis for Ligand Modulation of a Mammalian Voltage-Gated Ca(2+) Channel.* Cell, 2019. **177**(6): p. 1495-1506.e12.

46. Frasson, M., et al., *Retinitis pigmentosa: rod photoreceptor rescue by a calcium-channel blocker in the rd mouse.* Nat Med, 1999. **5**(10): p. 1183-7.

47. Fain, G.L. and J.E. Lisman, *Light, Ca2+, and photoreceptor death: new evidence for the equivalent-light hypothesis from arrestin knockout mice.* Invest Ophthalmol Vis Sci, 1999. **40**(12): p. 2770-2.

48. Olshevskaya, E.V., A.N. Ermilov, and A.M. Dizhoor, *Factors that affect regulation of cGMP synthesis in vertebrate photoreceptors and their genetic link to human retinal degeneration.* Mol Cell Biochem, 2002. **230**(1-2): p. 139-47.

49. Molday, R.S., *Calmodulin regulation of cyclic-nucleotide-gated channels.* Curr Opin Neurobiol, 1996. **6**(4): p. 445-52.

50. Cadetti, L., et al., *Calcium-induced calcium release in rod photoreceptor terminals boosts synaptic transmission during maintained depolarization.* Eur J Neurosci, 2006. **23**(11): p. 2983-90.

51. Johnson, M.T., et al., *L-type Ca2+; channel blockers promote vascular remodeling through activation of STIM proteins.* Proceedings of the National Academy of Sciences, 2020. **117**(29): p. 17369.

52. Saraiva, N., et al., *hGAAP promotes cell adhesion and migration via the stimulation of store-operated Ca2+ entry and calpain 2.* J Cell Biol, 2013. **202**(4): p. 699-713.

53. Bareil, C., et al., *Segregation of a mutation in CNGB1 encoding the beta-subunit of the rod cGMP-gated channel in a family with autosomal recessive retinitis pigmentosa.* Hum Genet, 2001. **108**(4): p. 328-34.

54. Wissinger, B., et al., *CNGA3 mutations in hereditary cone photoreceptor disorders.* Am J Hum Genet, 2001. **69**(4): p. 722-37.

55. Chen, T.Y., et al., *A new subunit of the cyclic nucleotide-gated cation channel in retinal rods.* Nature, 1993. **362**(6422): p. 764-7.

56. Hüttl, S., et al., *Impaired channel targeting and retinal degeneration in mice lacking the cyclic nucleotide-gated channel subunit CNGB1.* J Neurosci, 2005. **25**(1): p. 130-8.

57. Paquet-Durand, F., et al., *PKG activity causes photoreceptor cell death in two retinitis pigmentosa models.* J Neurochem, 2009. **108**(3): p. 796-810.

58. Wutz, K., et al., *Thirty distinct CACNA1F mutations in 33 families with incomplete type of XLCSNB and Cacna1f expression profiling in mouse retina.* Eur J Hum Genet, 2002. **10**(8): p. 449-56.

59. Krizaj, D. and D.R. Copenhagen, *Compartmentalization of calcium extrusion mechanisms in the outer and inner segments of photoreceptors.* Neuron, 1998. **21**(1): p. 249-56.

60. Spencer, M., P.B. Detwiler, and A.H. Bunt-Milam, *Distribution of membrane proteins in mechanically dissociated retinal rods.* Invest Ophthalmol Vis Sci, 1988. **29**(7): p. 1012-20.

61. Sanyal, S. and A.K. Bal, *Comparative light and electron microscopic study of retinal histogenesis in normal and rd mutant mice.* Z Anat Entwicklungsgesch, 1973. **142**(2): p. 219-38.

62. Mank, M., et al., *A FRET-Based Calcium Biosensor with Fast Signal Kinetics and High Fluorescence Change.* Biophysical Journal, 2006. **90**(5): p. 1790-1796.

63. Korschen, H.G., et al., *A 240 kDa protein represents the complete beta subunit of the cyclic nucleotide-gated channel from rod photoreceptor.* Neuron, 1995. **15**(3): p. 627-36.

64. Yu, W.P., M.E. Grunwald, and K.W. Yau, *Molecular cloning, functional expression and chromosomal localization of a human homolog of the cyclic nucleotide-gated ion channel of retinal cone photoreceptors.* FEBS Lett, 1996. **393**(2-3): p. 211-5.

65. Peng, C., et al., *Functionally important calmodulin-binding sites in both NH2- and COOH-terminal regions of the cone photoreceptor cyclic nucleotide-gated channel CNGB3 subunit.* J Biol Chem, 2003. **278**(27): p. 24617-23.

66. Liman, E.R., J. Tytgat, and P. Hess, *Subunit stoichiometry of a mammalian K+ channel determined by construction of multimeric cDNAs.* Neuron, 1992. **9**(5): p. 861-71.

67. Shammat, I.M. and S.E. Gordon, *Stoichiometry and arrangement of subunits in rod cyclic nucleotide-gated channels.* Neuron, 1999. **23**(4): p. 809-19.

68. Jonas, P., *High-speed solution switching using piezo-based micropositioning stages.*, in *Single-channel recording*, B. Sakmann and E. Neher, Editors. 1995, Plenum Press: New York. p. xxii, 700 p.

69. Thon, S., et al., *Conformational Flip of Nonactivated HCN2 Channel Subunits Evoked by Cyclic Nucleotides.* Biophys J, 2015. **109**(11): p. 2268-76.

70. Zheng, J. and W.N. Zagotta, *Patch-clamp fluorometry recording of conformational rearrangements of ion channels.* Sci STKE, 2003. **2003**(176): p. Pl7.

71. Nache, V., et al., *Differential regulation by cyclic nucleotides of the CNGA4 and CNGB1b subunits in olfactory cyclic nucleotide-gated channels.* Sci Signal, 2012. **5**(232): p. ra48.

72. Au - Belhadj, S., et al., *Long-Term, Serum-Free Cultivation of Organotypic Mouse Retina Explants with Intact Retinal Pigment Epithelium.* JoVE, 2020(165): p. e61868.

73. Hair, J.F., et al., *Multivariate data analysis New York.* NY: Macmillan, 1995.

74. Nobre, J.S. and J. da Motta Singer, *Residual analysis for linear mixed models.* Biom J, 2007. **49**(6): p. 863-75.

75. Kulkarni, M., et al., *Imaging Ca2+ dynamics in cone photoreceptor axon terminals of the mouse retina.* J Vis Exp, 2015(99): p. e52588.

76. Euler, T., et al., *Eyecup scope--optical recordings of light stimulus-evoked fluorescence signals in the retina.* Pflugers Arch, 2009. **457**(6): p. 1393-414.

77. Baden, T., et al., *A tale of two retinal domains: near-optimal sampling of achromatic contrasts in natural scenes through asymmetric photoreceptor distribution.* Neuron, 2013. **80**(5): p. 1206-17.

78. Nakagawa, S. and H. Schielzeth, *A general and simple method for obtaining R2 from generalized linear mixed-effects models.* Methods in Ecology and Evolution, 2013. **4**(2): p. 133-142.

ACKNOWLEDGEMENTS

We thank N. Rieger from the Tübingen Institute for Ophthalmic Research as well as K. Schoknecht, S. Bernhardt, A. Kolchmeier from Institute of Physiology II (Jena) for technical assistance. We thank also J. Kusch for excellent comments on the manuscript. This work was funded by the ProRetina Foundation and the Deutsche Forschungsgemeinschaft (DFG, German Research Foundation; PA1751/7-1, 8-1 to FPD; EU42/8-1 to TE; TRR 166 ReceptorLight project B01 and Project Number 437036164 to VN).

Author contributions

SD performed retinal explant cultures, TUNEL and immunostaining, microscopy, analysed data and helped write the manuscript; MP performed Ca^{2+}-imaging experiments; VP studied the effect of diltiazem on the CNGC activation and deactivation kinetics; KG performed colocalization experiments for heterotetrameric CNGC; CM performed molecular-biology work; MA performed immunostaining and analysed data; LR analysed Ca^{2+}-imaging data and performed statistical analysis; TS performed statistical analysis on immuno and bioassay data; FS synthesized fluorescent cGMP derivatives; VN performed electrophysiological and optical measurements to study the effect of diltiazem on retinal CNGC; VN, TE, and FPD designed the experiments, interpreted the data, and prepared the manuscript. All authors edited the manuscript.

SUPPLEMENTARY INFORMATION for:

Das et al.: Redefining the role of Ca^{2+}-permeable channels in hereditary photoreceptor degeneration using the D- and L-cis enantiomers of diltiazem

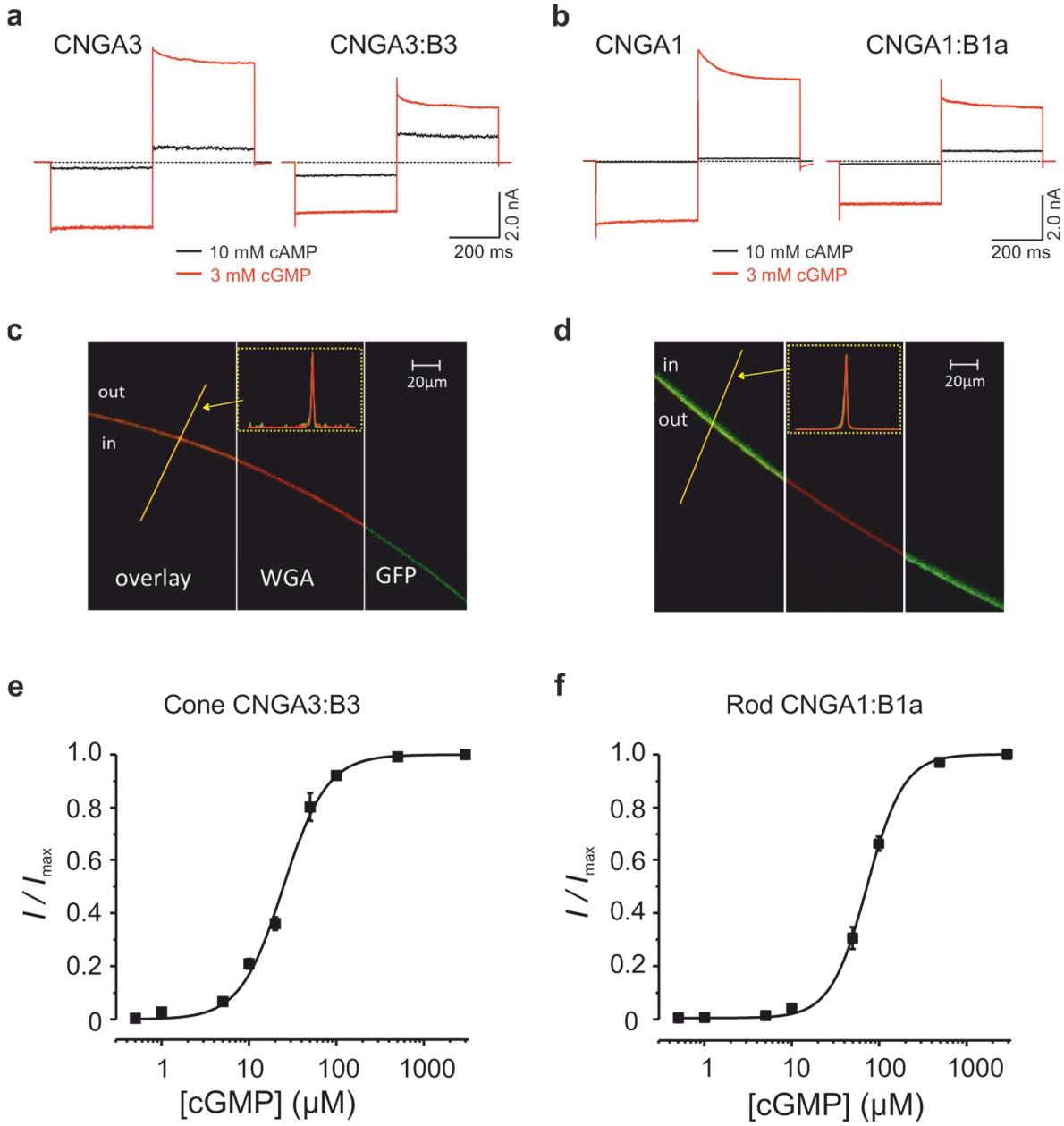

Supplementary Fig. 1: Functional properties of photoreceptor heterotetrameric CNGCs expressed in *Xenopus laevis* oocytes. Representative macroscopic cone (**a**) and rod (**b**) CNGC-current traces from inside-out membrane patches in the presence of 3 mM cGMP (red) and 10 mM cAMP (black). The current traces were elicited by voltage steps from a holding potential of 0 mV to -100, +100 and 0 mV. Leak currents in the absence of cGMP were subtracted for all recordings. For CNGA3 channels the ratio I_{cAMP}/I_{cGMP} was 0.15±0.01 (n=8). CNGB3-subunit incorporation into the CNGA3:B3

channel leads to a significant increase in the cAMP efficacy (I_{cAMP}/I_{cGMP}=0.42±0.03, n=6). Similarly, for CNGA1 channels the ratio I_{cAMP}/I_{cGMP} was 0.019±0.005 (n=12), whereas for heterotetrameric CNGA1:B1a channels the ratio was 0.16±0.02 (n=6). (**c, d**) Representative measurements showing confocal images of oocyte membrane expressing heterotetrameric CNGA3:B3-GFP (**c**) and CNGA1:B1a-GFP (**d**) channels (green fluorescence signal). The oocyte plasma membrane was labelled with Alexa Fluor™ 633 WGA (red fluorescence signal). The small insets show fluorescence profiles along the yellow line, perpendicular to the membrane and confirm the colocalization of the labelled channels with the oocyte membrane. For each channel isoform we tested more than 10 oocytes from at least two different oocyte batches. (**e**, **f**) cGMP-dependent concentration-activation relationships for cone CNGA3:B3 (**e**) and rod CNGA1:B1a (**f**) channels obtained at -35 mV. The currents triggered by subsaturating ligand concentrations were normalized with respect to the maximal current at 3 mM cGMP. The experimental data points, each representing the mean of 5 to 10 measurements, were fitted with Eq. (1). The parameters obtained are included in Table 1.

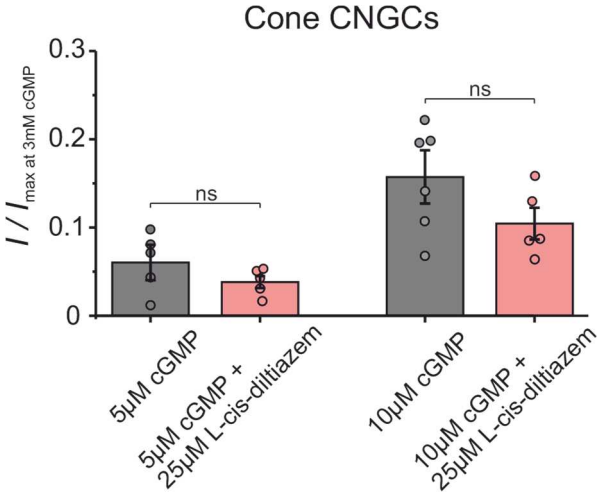

Supplementary Fig. 2: L-cis-diltiazem does not influence the activity of cone CNGCs under physiological conditions. The normalized cone CNGC currents were triggered by either 5 µM or 10 µM cGMP (black columns) in the presence and in the absence of 25 µM L-cis-diltiazem (light-red columns). The measurements were performed under steady-state conditions, at -35 mV. We observed no statistical difference between the experiments with and without the blocker. The results obtained with the two-tailed unpaired Student *t*-test were the following: (1) for 10 µM cGMP and 10 µM cGMP + 25 µM L-cis-diltiazem the p-value was 0.1667; (2) for 5 µM cGMP and 5 µM cGMP + 25 µM L-cis-diltiazem the p-value was 0.2256.

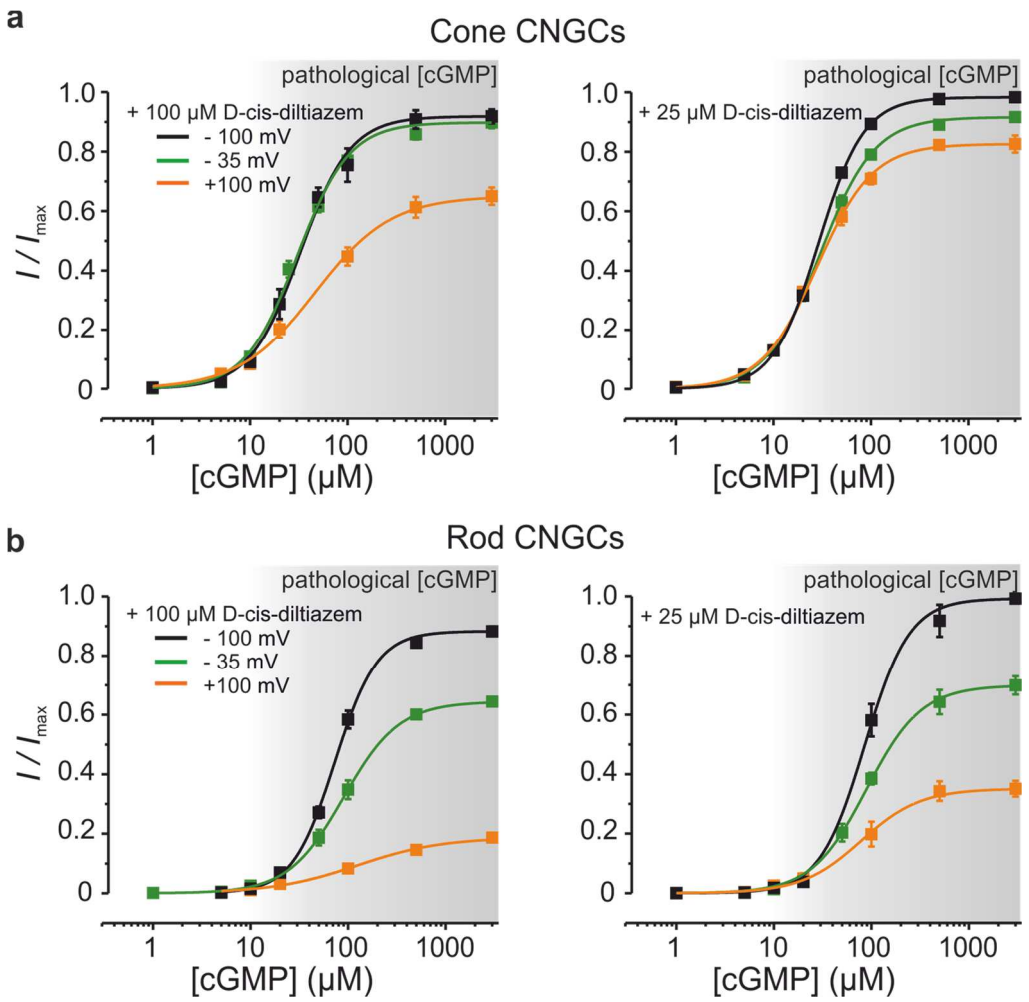

Supplementary Fig. 3: Voltage dependence of D-cis-diltiazem-induced inhibition of photoreceptor CNGCs. (**a, b**) cGMP-dependent concentration-activation relationships for cone (**a**) and rod (**b**) CNGCs in the presence of 100 µM (left) and 25 µM (right) D-cis-diltiazem, measured at: -100 mV (black symbols), -35 mV (green symbols) and +100 mV (orange symbols). The current amplitudes were normalized with respect to the saturating currents measured in the absence of diltiazem at each individual voltage. The experimental data points were fitted with the Hill equation (Eq. 1). All parameters obtained from the fits are included in Table 1.

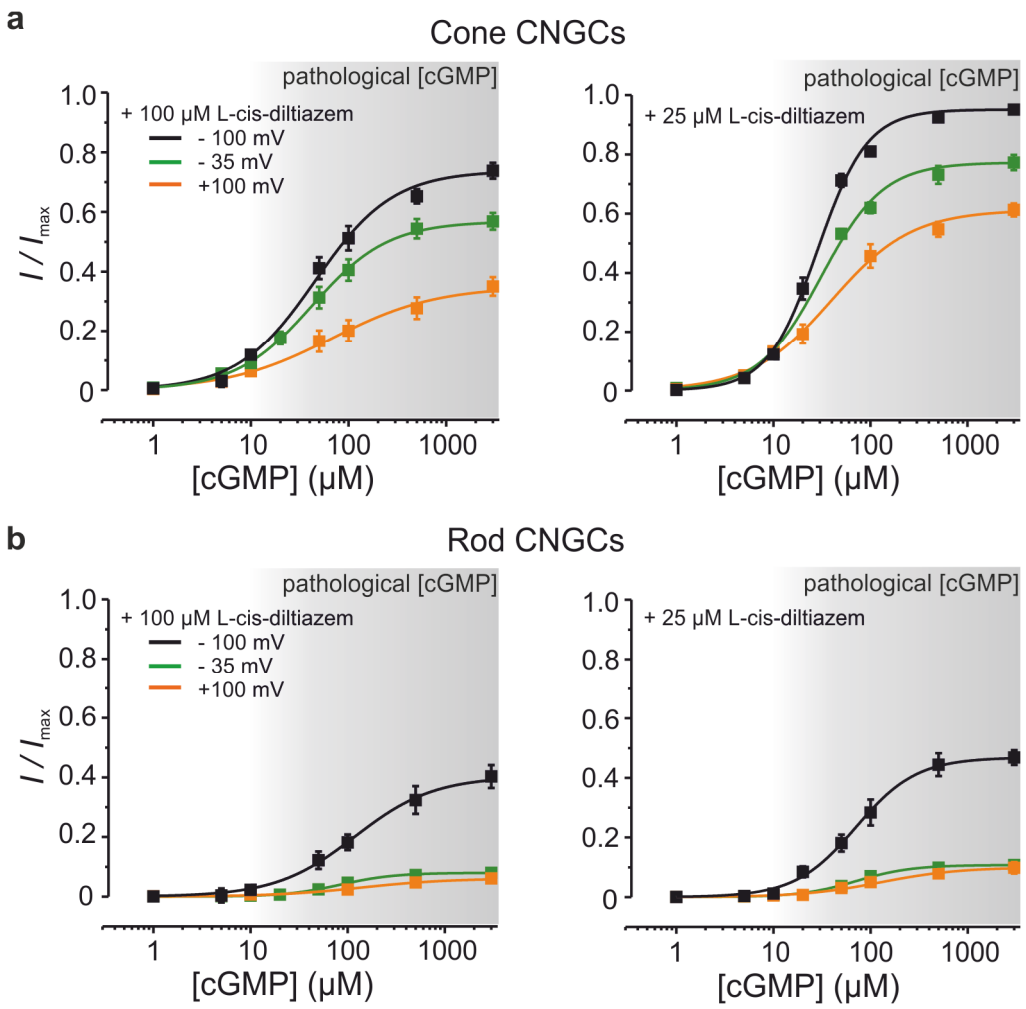

Supplementary Fig. 4: Voltage dependence of L-cis-diltiazem-induced inhibition of photoreceptor CNGCs. (**a, b**) cGMP-dependent concentration-activation relationships for heterotetrameric cone (**a**) and rod (**b**) CNGCs in the presence of 100 µM (left) and 25 µM (right) L-cis-diltiazem, measured at: -100 mV (black symbols), -35 mV (green symbols) and +100 mV (orange symbols). The current amplitudes were normalized with respect to the saturating currents measured in the absence of diltiazem at each individual voltage. The experimental data points were fitted with the Hill equation (Eq. 1). All parameters obtained from the fits are included in Table1.

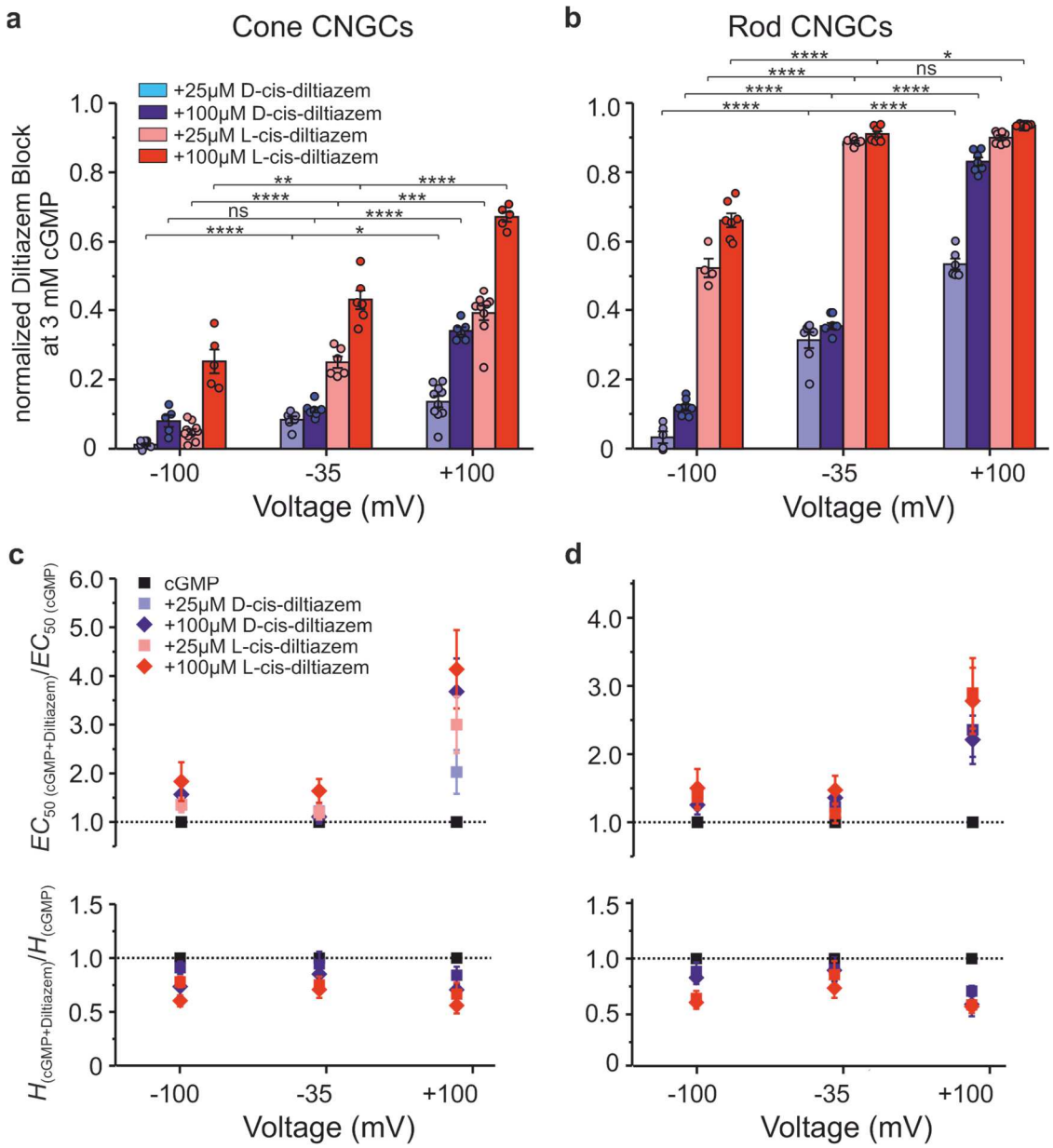

Supplementary Fig. 5: Differential effect of D-cis- and L-cis-diltiazem on CNGC's activity and apparent affinity. (**a, b**) D- and L-cis-diltiazem - block of cone and rod CNGCs activity triggered by saturating cGMP at three different voltages. The amount of diltiazem block was calculated using Eq. 2. (**c, d**) Effect of D- and L-cis-diltiazem on the channel's apparent affinity. Shown are the $EC_{50,(cGMP+Diltiazem)}/EC_{50,(cGMP)}$- and $H_{(cGMP+Diltiazem)}/H_{(cGMP)}$- ratios in the presence of 25 µM or 100 µM D- or L-cis-Diltiazem at -100 mV, -35 mV and +100 mV. The EC_{50}- and H-values were obtained from the concentration-activation relationships shown in Fig. 1 and Supplementary Figs. 3,4 (see also Table 1). For the statistical analysis on of the effect of diltiazem on EC_{50}- and H-values see Supplementary Table 1.

mV	cone CNGC:				*p*-value			
	cGMP + 25µM D-cis-diltiazem		cGMP + 100 µM D-cis-diltiazem		cGMP + 25µM L-cis-diltiazem		cGMP + 100 µM L-cis-diltiazem	
	EC_{50}	*H*	EC_{50}	*H*	EC_{50}	*H*	EC_{50}	*H*
-35	0.04242	ns	ns	ns	ns	0.00677	0.00277	0.00295
-100	0.00042	ns	0.000527	0.00934	0.000291	0.00121	0.000153	<0.0001
+100	0.000151	ns	0.00103	0.01494	0.00222	ns	0.01297	0.00636
	rod CNGC:				***p*-value**			
-35	ns	ns	0.02422	ns	ns	ns	0.02159	0.02111
-100	0.00534	ns	0.04734	ns	0.01729	0.00055	ns	0.00012
+100	<0.0001	<0.0001	<0.0001	<0.0001	<0.0001	<0.0001	<0.0001	<0.0001

Supplementary Table 1: Statistical analysis of the effect of diltiazem on CNGC EC_{50}- and *H*-values at different voltages. The respective parameters and number of experiments are listed in Table 1. The EC_{50} and *H*-values in the presence of cGMP only were compared with the respective values in presence of cGMP and diltiazem.

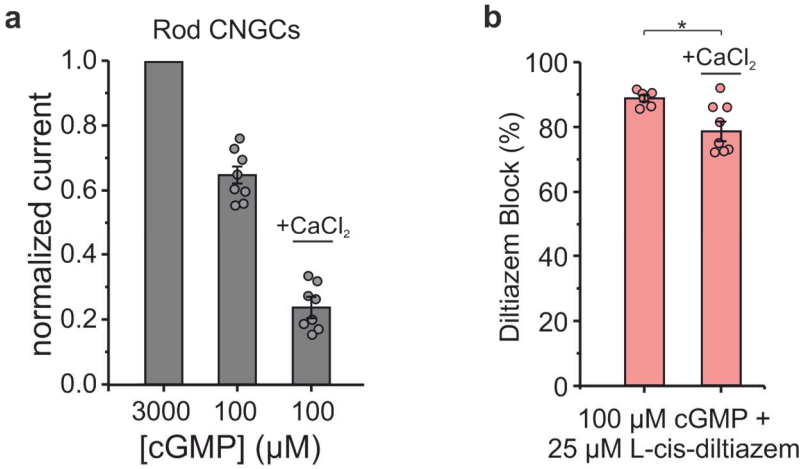

Supplementary Fig. 6: Effect of Ca^{2+} on the blocking effect of L-cis-diltiazem on rod CNGCs. (**a**) The diagram shows normalized rod CNGCs current triggered by 100 µM cGMP, in the absence and in the presence of 1 mM $CaCl_2$ in the extracellular solution. The current at 100 µM was normalized with respect to the current in the presence of 3 mM cGMP, under the respective $CaCl_2$-conditions (n=9). The channel response to cGMP is much weaker in the presence of Ca^{2+} ($I_{cGMP+CaCl2}/I_{max}$ = 0.233±0.03) as it is in its absence (I/I_{max} = 0.65±0.026). (**b**) L-cis-diltiazem - block of rod CNGC activity triggered by 100 µM cGMP in either the presence or absence of Ca^{2+}. The amount of diltiazem block was calculated using Eq. 2. The two-tailed unpaired Student *t*-test was used for the statistical analysis: **p*=0.034.

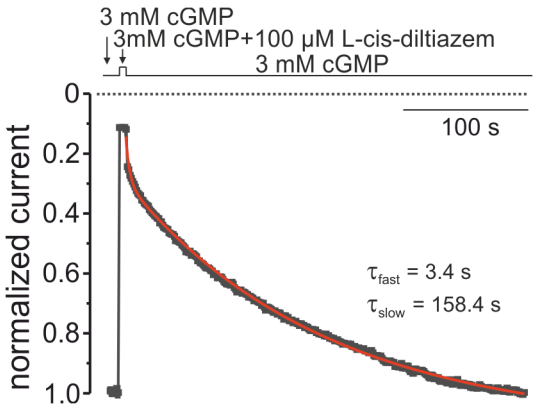

Supplementary Fig. 7: Kinetics of L-cis-diltiazem removal. Normalized rod CNGC current triggered by 3 mM cGMP, before, during and after the removal of 100 µM L-cis-diltiazem. The current trace represents the mean of 5 measurements. The individual data points (black symbols) were connected by lines and were obtained under steady-state conditions, at -35 mV. The experimental protocol is depicted on top of the diagram. The time course of current recovery, which mirrors the L-cis-diltiazem removal, was fitted by a double-exponential function (red line, Eq. 4) yielding the following time constants: τ_{fast} = 3.4 s and τ_{slow} = 158.4 s.

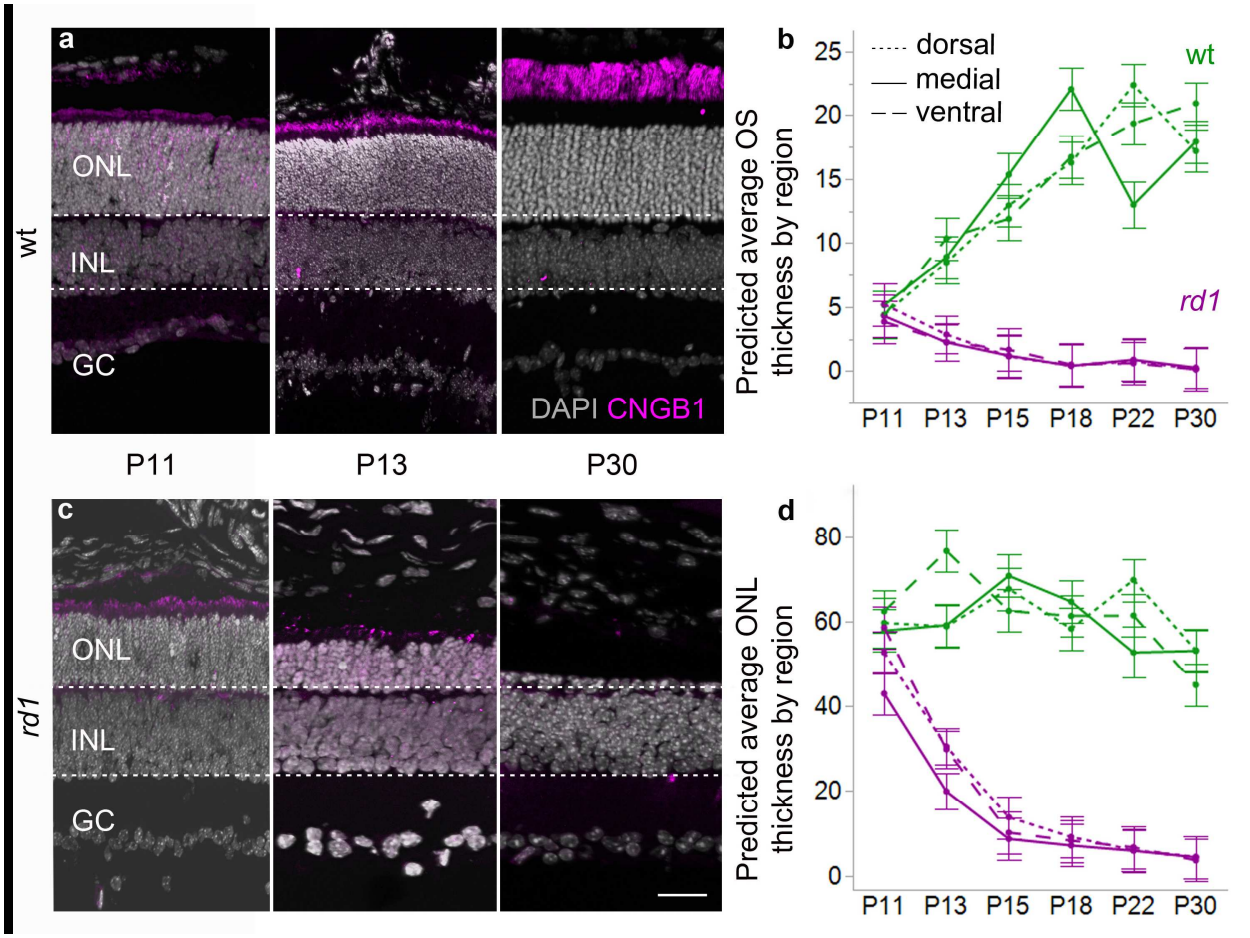

Supplementary Fig. 8: ONL thickness and CNGC expression during *rd1* retinal degeneration. Immunostaining for CNGB1a (magenta) was performed at different post-natal (P) days in wild-type (wt) and *rd1* retina (a,c). The nuclear counterstain (DAPI, grey) indicates outer nuclear layer (ONL), inner nuclear layer (INL), and ganglion cell layer (GC). Dotted, solid and dashed lines in the graph represent dorsal, medial, and ventral mouse retina respectively (b,d). (**a**) In wt retina, CNGB1a immunostaining labelled the photoreceptor outer segments, which grew longer from P11 to P30. (**c**) In *rd1* retina, CNGB1a positive outer segments were visible at P11 and P13 but essentially disappeared by P30. (**d**) The thickness of the ONL in wt retina (green) remained approx. constant between P11 and P30, while *rd1* (magenta) ONL size rapidly diminished after P11. (**b**) Outer segments in wt retina grew longer from P11 to P24 until reaching a plateau at a length of approx. 20 µm. In contrast, *rd1* outer segments, while still comparable to wt at P11, had decreased in length to nearly 0 µm by P24. Images and quantification were obtained from retinal sections from 4-5 different animals per time-point and genotype. Scale bar = 30 µm.

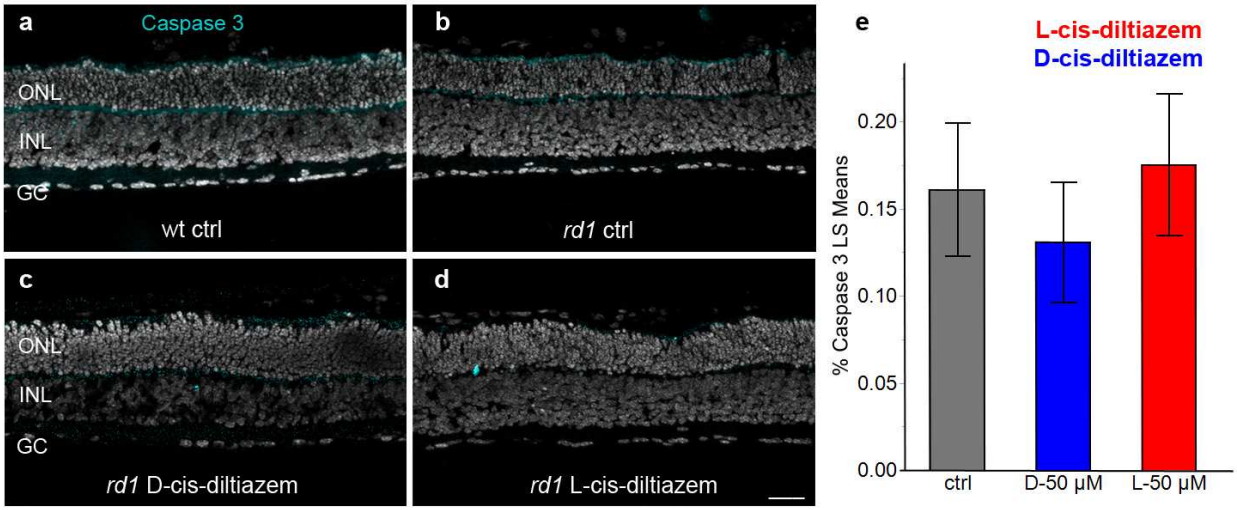

Supplementary Fig. 9: Absence of apoptotic marker during photoreceptor degeneration. Immunostaining for cleaved, activated caspase-3 (turquoise) was performed on *rd1* retinal sections treated with D- and L-cis-diltiazem (50 µM). While caspase-3 immunoreactivity was occasionally found in both outer and inner nuclear layer (ONL, INL), the percentage of caspase-3 positive cells was far lower than the numbers of dying cells (*cf.* Fig. 6). Scale bar = 50 µm.